J. Fluid Mech. (1971), *vol.* 45, *part* 3, *pp.* 477–512
Printed in Great Britain

A study of free jet impingement. Part 2. Free jet turbulent structure and impingement heat transfer

By COLEMAN DUP. DONALDSON, RICHARD S. SNEDEKER AND DAVID P. MARGOLIS
Aeronautical Research Associates of Princeton, Inc., Princeton, New Jersey

(Received 12 November 1968 and in revised form 29 May 1970)

An experimental study of jet impingement is completed with the presentation of the measured turbulent characteristics of the circular subsonic jet and the heat transfer rates measured when this jet impinges normal to a flat plate. The data suggest that for impingement very close to the stagnation point, the heat transfer can be computed by applying a turbulent correction factor to the laminar value calculated for a flow having the same pressure distribution as that present in the impingement region. The correction factor is found to be a function of the axial distance and not of Reynolds number. Farther away, the measurements agree well with the heat transfer estimated using the method of Rosenbaum & Donaldson (1967). At large distances from the stagnation point, the heat transfer falls off in inverse proportion with the distance.

The documentation of the turbulent jet flow field includes measurements of the radial and axial velocity fluctuations and their spectra, as well as the radial distribution of turbulent shear $\overline{w'u'}$. In addition, measurements of the turbulence near the stagnation point and the total pressure fluctuation at the stagnation point are presented.

1. Introduction

The research that will be described in this paper is the second part of a general study of the relationship between the local properties of axially symmetric free jets and the flows that result when such jets impinge upon a surface (Donaldson & Snedeker 1971). One objective of this total programme has been to gain an understanding of the heat transfer that results when the temperature of such a jet is different from that of the surface upon which it impinges.

If a laminar free jet impinges normally on a flat plate and if the flow is steady, the stagnation point heat transfer can be computed if one has a knowledge of the molecular transport properties of the gas in question, the centreline stagnation enthalpy of the jet, the temperature of the plate, and the pressure distribution in the region of impingement. The computation can be made since exact solutions of the Navier–Stokes equations can be obtained for laminar stagnation points. The key to obtaining such a solution is a knowledge of the stagnation point velocity gradient. For most Reynolds numbers of interest, this parameter may be determined from the measured pressure distribution in the region of impingement. Much attention has been given in the paper referred to above to relating

this heat transfer parameter to the local mean properties that a free jet would have in the plane of impingement if the surface on which impingement takes place were removed.

Unfortunately, most free jets of practical importance are not laminar but are turbulent, and we are led to the problem of the effect of turbulence on stagnation point heat transfer. Over the past twenty years, a number of studies have been carried out on the effects of free stream turbulence on heat transfer (Reiber 1925; Comings, Clapp & Taylor 1948; Maisel & Sherwood 1950; Giedt 1949; Zapp 1950; van der Hegge Zijnen 1957; Schnautz 1958; Seban 1960; Kestin, Maeder & Sogin 1961; Smith & Kuethe 1966). The most recent of these studies has considered in detail the heat transfer in the vicinity of the stagnation line of cylinders placed normal to a turbulent air stream. In general, for relative turbulent intensities that are less than 10 percent and for cylinders (two-dimensional flow), it has been found that stagnation heat transfer increases linearly with turbulence intensity, with the slope of this linear increase being larger with increase in Reynolds number. Unfortunately, there are large discrepancies among the slopes found by various investigators. The data are not sufficiently complete to enable the cause of these discrepancies to be determined at the present time, although it has been demonstrated (van der Hegge Zijnen 1957) that the ratio of the integral scale of the turbulence to the diameter of the cylinder can be an important additional parameter.

In the case of heat transfer to spheres (axisymmetric flow), there is not so much information, but that which exists in the literature indicates that the effect of turbulence on stagnation point heating for small turbulence levels is less in axisymmetric flow than it is in two-dimensional flow. In spite of all the quantitative uncertainty which is found in the data, it does appear that the best method of handling the computation of stagnation point heating in the presence of turbulence is to compute the normal laminar stagnation point heat transfer rate and then to apply a correction factor which is a function of the free stream turbulence level, an appropriate Reynolds number, and the ratio of the integral scale of the turbulence to the length used in defining Reynolds number. Correction factors as high as 1·8 for turbulence levels as low as 2·7% have been reported in the literature (Kestin *et al.* 1961).

In considering the heat transfer to a surface due to the impingement of a turbulent jet, it was decided in the present study that the correction factor method should be used in trying to correlate the stagnation point heat transfer rates which were to be measured. To adopt this approach required that detailed measurements of the turbulent character of the jet studied in Donaldson & Snedeker (1971) be made. Thus a considerable portion of this report will be devoted to the determination of the jet microstructure.

In addition to the usual measurements of turbulent velocity correlations and their spectra, measurements were also made of the fluctuation of total pressure on the centreline of the free jet and at the stagnation point for the case of jet impingement.

Since we are primarily interested in the distribution of heat transfer under an impinging free jet, the remainder of the results are concerned with measurements

of the heat transfer from a heated flat plate to a cooler jet which impinges normally. In particular we will, following the procedure of Donaldson & Snedeker (1971), attempt to correlate the resulting local heat transfer rates with the properties of the free jet in the plane of impingement, an appropriate local temperature difference, and the distance from the point of impingement made non-dimensional with respect to the half-radius r_5 of the free jet in the plane of impingement. (The half-radius is the radius at which the velocity has one-half its maximum value.)

Before going on to present these results, a review of some previous work on impingement heat transfer is in order. Until quite recently, very little information on the details of jet impingement heat transfer existed. However, within the past decade several most useful studies have been made. Vickers (1959) studied the local heat transfer coefficients due to a laminar axisymmetric fluid jet impinging normally on a flat surface. Results are presented for Reynolds numbers based on the jet exit velocity and diameter from 250 to 950 and for non-dimensional impingement distances $8 < z/d_N < 20$, where z is the axial distance and d_N is the jet exit diameter. Gardon & Cobonpue (1961) measured local heat transfer coefficients for both single and multiple circular turbulent jets. Reynolds numbers varied from 7×10^3 to $1{\cdot}12 \times 10^5$ and the range of z/d_N studied was $1{\cdot}5 < z/d_N < 50$. It is interesting to note the variation of stagnation point heat transfer with z/d_N reported in this work for single jets. In figure 1 (*a*) we have reproduced the pertinent figure from Gardon & Cobonpue's paper. Note the large variation in heat transfer between $z/d_N = 1{\cdot}5$ and $z/d_N = 15$. This is primarily due to the variation in the stagnation point velocity gradient $(du_e/dr)_{r=0}$ as a result of the elimination of the potential core and formation of a developed jet. This may be seen by comparing the results shown in figure 1 (*a*) with the results shown in figure 1 (*b*) which is taken from Donaldson & Snedeker (1971).

Huang (1963) also studied the heat transfer below an impinging axially symmetric jet. Measurements were made for impingement distances from $z/d_N = 1$ to $z/d_N = 12$ and for the region $0 < r/d_N < 20$. Jet Reynolds numbers were varied from 10^3 to 10^4. Huang does not indicate a variation of stagnation point heat transfer coefficient with z/d_N for the range $1 < z/d_N < 12$ where significant variations were observed by Gardon & Cobonpue. This result is probably due to the lower Reynolds numbers at which these data were taken, as might be expected from an inspection of figure 1 (*a*).

Gardon & Akfirat (1965*a*, *b*) report measurements of local heat transfer below two-dimensional slot jets impinging on a flat plate. The range of Reynolds numbers (based on slot velocity and slot breadth b_N) was from 450 to 50,000. These data show the rapid variation of heat transfer with z/b_N in the range $1 < z/b_N < 15$ due to the elimination of the potential core and formation of a developed jet, as has been discussed above. The effect, however, appears to be somewhat more pronounced in two-dimensional jets than it is in axisymmetric jets. Of considerable importance is the observation by Gardon & Akfirat that increasing the initial turbulence level of the jet increased the stagnation point heat transfer in the core region ($z/d_N \cong 2$). In particular, by increasing the turbulence intensity from 2·5%

to 6 and 18% through the use of turbulence promoters, the heat transfer was increased over its value for 2·5% intensity by 1·2 and 1·7 times, respectively.

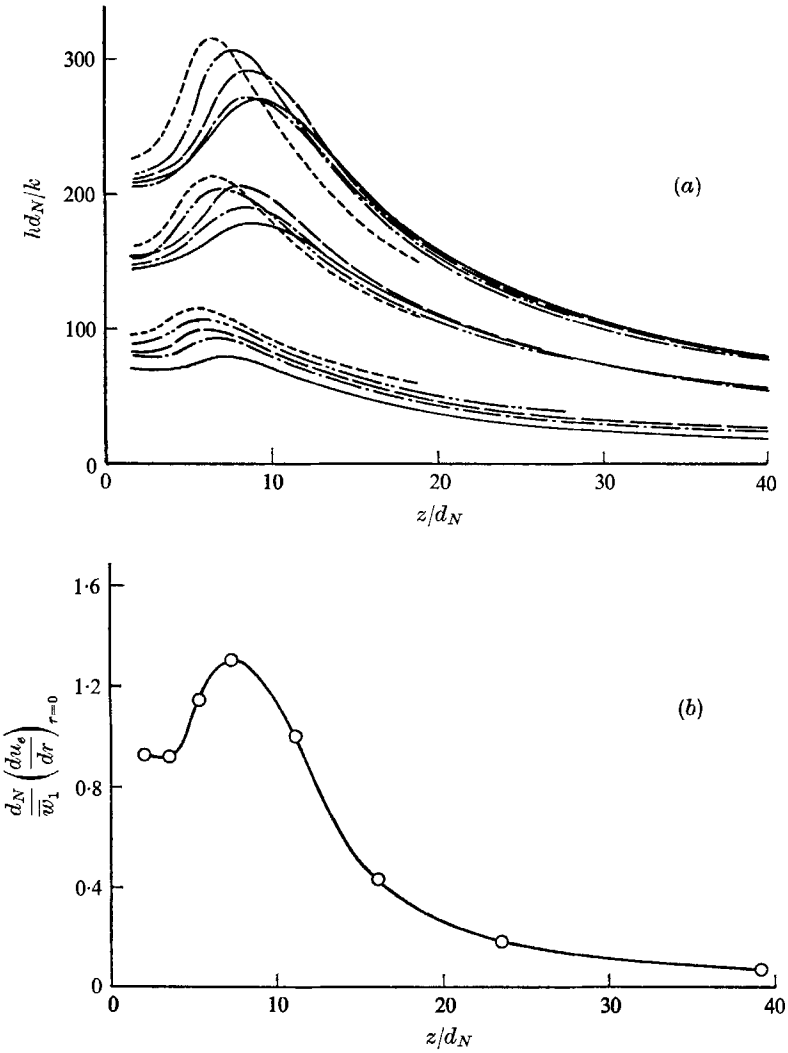

FIGURE 1. (*a*) Stagnation point heat transfer measured by Gardon & Cobonpue (1961). Sets of curves from top to bottom, $Re_d = 56 \times 10^3$, 28×10^3, 7×10^3. Values of nozzle diameter d_N in inches: ——, 0·089; — · —, 0·125; — —, 0·177; — · · —, 0·250; · · · · · ·, 0·354. (*b*) Measured stagnation point velocity gradients from Donaldson & Snedeker (1971). $\overline{w}_1 = 665$ ft./sec, $d_N = 0{\cdot}511$ in.; $Re_d = 147 \times 10^3$.

O'Connor, Comfort & Cass (1965) have measured the heat transfer below an impinging arc jet at distances such that $6 < z/d_N < 20$ and at Reynolds numbers from 8×10^3 to $1{\cdot}8 \times 10^4$. In this work a detailed study of the mean structure of the free jet was carried out so that the stagnation point heat transfers might be compared with appropriate computations made for a laminar stagnation point having the same velocity gradient $(du_e/dr)_{r=0}$. The result when such a

comparison was made was that the theoretical prediction was low by a factor of about 2.

The factor of 2 found by O'Connor *et al.* is, as will be seen in what follows, roughly equal to the factor found in the measurements reported here for fully developed jets. According to the philosophy that has been adopted, this factor must be ascribed to the existence of turbulence in the fully developed impinging jet.

As found in the studies referred to above, the general character of the heat transfer that results from impinging jets is quite dependent on the jet Reynolds number as well as the position of impingement relative to the core. For fully developed jets, the stagnation point heat transfer is found to be proportional to the square root of the local free jet Reynolds number $Re_5 = \rho_c \overline{w}_c r_5/\mu_c$ times a factor of the order of unity which accounts for the effect of jet turbulence. In this expression, ρ_c, $\overline{w}_c$, and μ_c are the local density, mean axial velocity, and viscosity, respectively, all evaluated on the jet centreline. Away from the stagnation point, under the wall jet which develops on the impingement surface, the heat transfer is found to be proportional to the eight-tenths power of the local free jet Reynolds number. The different dependence of these two heat transfers on Reynolds number causes the relative magnitudes of stagnation point heat transfers and wall-jet heat transfers to vary over wide ranges with Reynolds number. A plot of the Nusselt number $\dot{q}r_5/k\Delta T$ divided by the eight-tenths power of the Reynolds number Re_5 versus r/r_5 for several values of Re_5 has, in general, the character shown in figure 2. Note that for small Reynolds number the stagnation point heat transfer is large compared to the wall-jet heat transfer and one observes a monotonic drop-off of heat transfer with radius.† When the Reynolds number is large, on the other hand, the stagnation point heat transfer is small compared to the wall-jet heat transfer, and one observes an initial rise in heat transfer as r/r_5 increases before observing the usual fall-off at large r/r_5. In the experiments that will be discussed in this paper, the Reynolds number was such that the break in the curve that occurs on transition from laminar to turbulent flow is so small as to be obscured by the scatter of the experimental data.

2. Experimental apparatus and technique

2.1. *General description*

The jet apparatus used in these experiments was the same as that used in the earlier studies performed at ARAP on free and impinging jets (Donaldson & Snedeker 1971). The jet was produced by a convergent nozzle with an exit diameter of 0·511 in. using air supplied from a blow-down system. Supporting hardware for the probes and impingement surfaces was designed to produce a minimum of interference with the jet flow field.

Pertinent details of the apparatus, instrumentation, and techniques used in measuring the turbulence, fluctuating pressure, and heat transfer characteristics of the jet are given in the following sections.

† This behaviour is found provided the impingement takes place sufficiently far from the nozzle so that nozzle interference effects are not present.

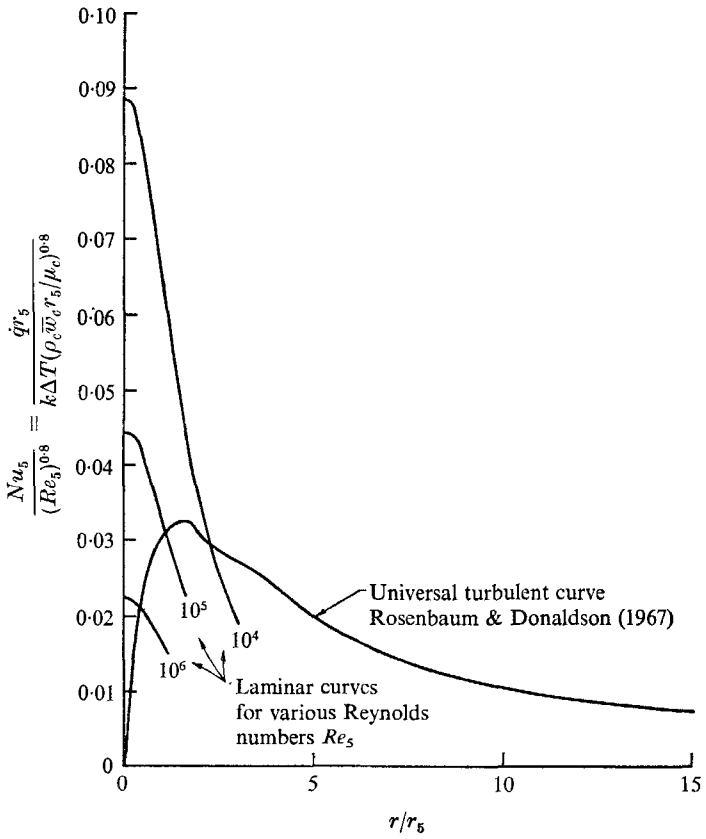

FIGURE 2. General character of jet impingement heat transfer as a function of distance from the stagnation point.

2.2. *Free jet turbulence measurements*

Measurements of the turbulence intensities and shear stress in the free jet were made using a Thermo-Systems linearized, constant temperature, hot-film anemometer. A block diagram of this instrumentation is shown in figure 3. The basic elements in this system are two Model 1010 Thermo-Systems anemometers with two Model 1035 linearizers. An X-probe was used with 0·001 in. diameter platinum film sensors. The sum-difference network and the electronic integrator were designed and built at ARAP.

One-dimensional energy spectra of $\overline{w'^2}$ (axial component) and $\overline{u'^2}$ (radial component) were measured on the jet centreline using a Hewlett Packard Model 302 A wave analyzer. The analyzer has a fixed effective bandwidth of 8 Hz and a range of 20–50,000 Hz.

Radial surveys were made by traversing the probe across the jet from edge to edge in a vertical plane through the jet centreline. The measurements of turbulent shear stress were made by traversing the jet twice, once with the probe in its 'normal' position and once with the probe 'inverted' or rotated about its axis 180°. The average of the two profiles produced was taken to represent the actual

measured shear stress distribution. This technique serves, in an axisymmetric flow, to eliminate the error caused when X-probe sensors have different angles relative to the mean flow as long as the axis about which the probe is rotated is parallel to the mean flow. In this case, the probe shaft was parallel with the jet centreline within 0·2°. In these measurements, no corrections were made for intermittency or non-linear sensor response.

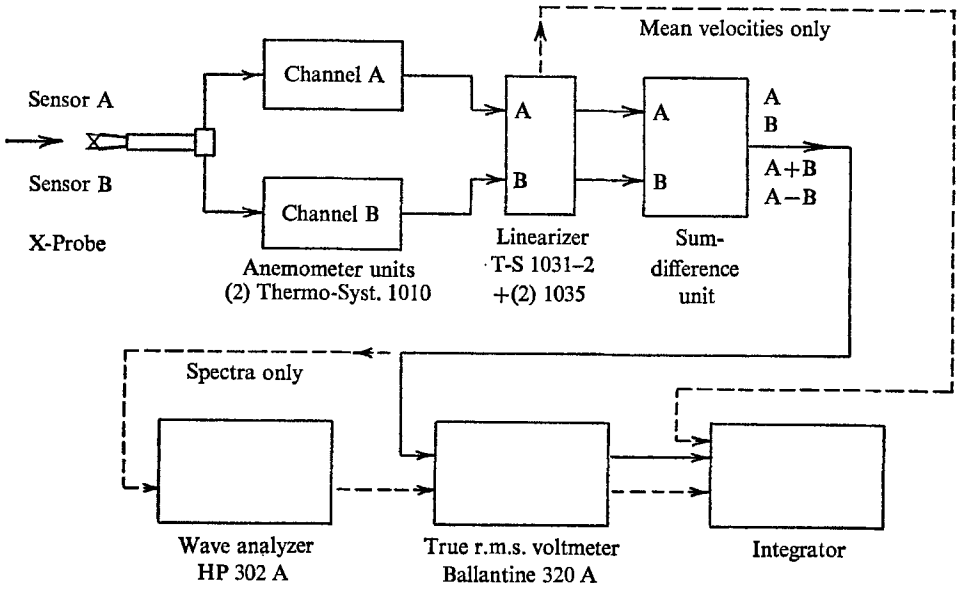

FIGURE 3. Block diagram of turbulence measuring equipment.

2.3. *Measurements of fluctuating stagnation pressure*

The measurement of fluctuating stagnation pressure levels in the free and impinging jet was accomplished using a Bruel and Kjaer condensor microphone Model 4136 with matching cathode follower and microphone amplifier Model 2603. Signals from the microphone amplifier were fed to the wave analyzer and integrating circuitry used in the turbulence measurements.

Pressure level measurements were made on the centreline of the free and impinging jets by exposing the microphone diaphragm to the oncoming flow through a small probe tube. The probe tube and the microphone enclosure are shown in figure 4. Because of the exposure of the front surface of the microphone diaphragm to the full dynamic pressure of the flow, it was necessary to provide an additional path to allow for the equalization of the mean pressure on the front and rear surfaces of the diaphragm. To accomplish this, an outer concentric tube was mounted around the inner microphone tube and connected to a chamber within the microphone enclosure which led to the equalization hole at the rear of the cartridge. The chamber itself was sealed from the static pressure outside the enclosure with an 'O' ring. The inner tube was mounted in a solid B & K 4136 grid cap (i.e. one without slots) which facilitated attachment to the cartridge. The natural frequency of the outer tube, considered as a cantilever and without the stiffening effect of the inner tube, was calculated to be about 24,000 Hz, well

above the range of interest. The theoretical fundamental 'organ pipe' resonant frequency of the inner tube was about 3400 Hz. Although this falls within the range of interest, its presence could not be detected during either the probe calibrations or the spectral measurements.

Because of the non-uniform frequency response of the probe tube, it was necessary to determine the overall fluctuating pressure levels by making spectral measurements and integrating them over the range of interest after applying a probe tube correction at each frequency. The required frequency response characteristics were determined by mounting the probe with its tube through the wall of a 2-cubic centimetre coupling chamber containing a calibrated sound source.†

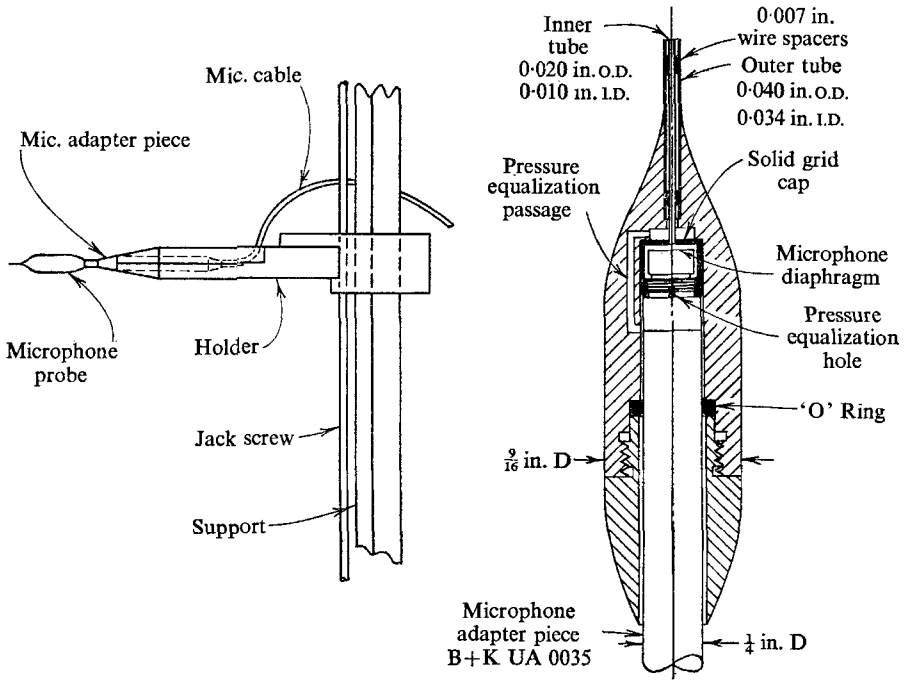

FIGURE 4. Microphone mounting assembly and probe detail.

For the measurements in the free jet, the microphone was clamped rigidly on the traversing mechanism. The impinging jet measurements were performed using the same microphone probe assembly, but with the probe tube fitted snugly into a hole at the centre of a $\frac{1}{2}$ in. thick aluminium plate and positioned flush with the surface. The adapter piece and cathode follower were supported rigidly at the rear of the plate. The plate itself was held in the adjustable mounting jig shown in figure 6 (plate 1).

2.4. *Heat transfer measurements*

The measurements of convective heat transfer coefficients were made with the cold jet impinging on a flat, circular, heated plate containing 14 flush-mounted calorimeter disks with thermocouples attached. The initial portion of the recorded

† The authors wish to thank Professor E. G. Wever and members of the staff of the Auditory Research Laboratory at Princeton University for their help in performing this calibration.

temperature–time response of each thermocouple was used to determine the heat transfer at that point by matching the response with a suitable analytical expression.

In the design of the plate, the usual considerations for establishing the most valid behaviour of the calorimeters were taken into account (see, e.g. Westkaemper 1960, 1961; Wehofer 1963). That is, both lateral conduction and thermal resistance normal to the surface were minimized. The heat transfer plate and the calorimeter gauges were made of copper sheet 0·015 in. thick. The plate was 12 in. in diameter and was bonded to an insulating back-up plate of rigid polyurethane foam 1 in. thick (see figure 5). The foam used was Emerson and Cuming 'Eccofoam SH' with a density of 8 lb./ft.^{3}. The copper was bonded to the foam using a high temperature epoxy adhesive, Emerson and Cuming 'Eccobond 106'.

The calorimeter disks were $\frac{3}{16}$ in. in diameter with a copper-constantan thermocouple junction at the centre. Each calorimeter was insulated from the plate surrounding it by a $\frac{1}{32}$ in. wide ring of epoxy foam (Emerson and Cuming 'Eccofoam DPT'). The finished plate contained eight pressure taps for use in aligning the plate in the flow.

A heater was designed which could be held against the surface of the test plate and then removed suddenly when the surface reached the desired temperature. This heater consisted of a circular, buried-element, electric heating pad of silicone rubber, bonded to a backing plate of 'Eccofoam SH'. The heating pad was manufactured by Watlow Electric Company. The heater assembly was mounted on the end of a pivoted arm so that it could be removed quickly from the vicinity of the plate. Another pivoted arm was used to deflect the jet stream until after the heater was removed.

The output of each thermocouple was recorded directly on a Model 906C Honeywell 'Visicorder' oscillograph. The thermocouple cold reference junction was maintained at 32 °F in an ice bath, and the response of the oscillograph galvanometers was calibrated using a separate thermocouple junction at the same point in the circuit at which the gauges were finally attached.

Two views of the complete heat transfer apparatus are shown in figure 6 (plate 1).

Calibration of heat transfer gauges. Prior to assembly of the heat transfer plate, the desired response of the gauges was verified by tests using a radiant heat input to produce a predictable gauge response. For this purpose, a single gauge assembly was made and mounted exactly as were the 14 gauges in the plate. The copper sheet surrounding the gauge was 2 in. square. Another gauge, identical but unmounted, was also prepared in order to measure the heat input. This gauge was blackened with lampblack to ensure an emissivity of unity. It was held only by its thermocouple leads and exposed to the concentrated beam of three infra-red heat lamps.

It was assumed that the response of the calibration gauge was governed by the following differential equation

$$mc_p \frac{dT_w}{dt} = \dot{q}_{\text{in}} - hA_c(T_w - T_0) - \sigma\epsilon A_r(T_w^4 - T_0^4), \tag{1}$$

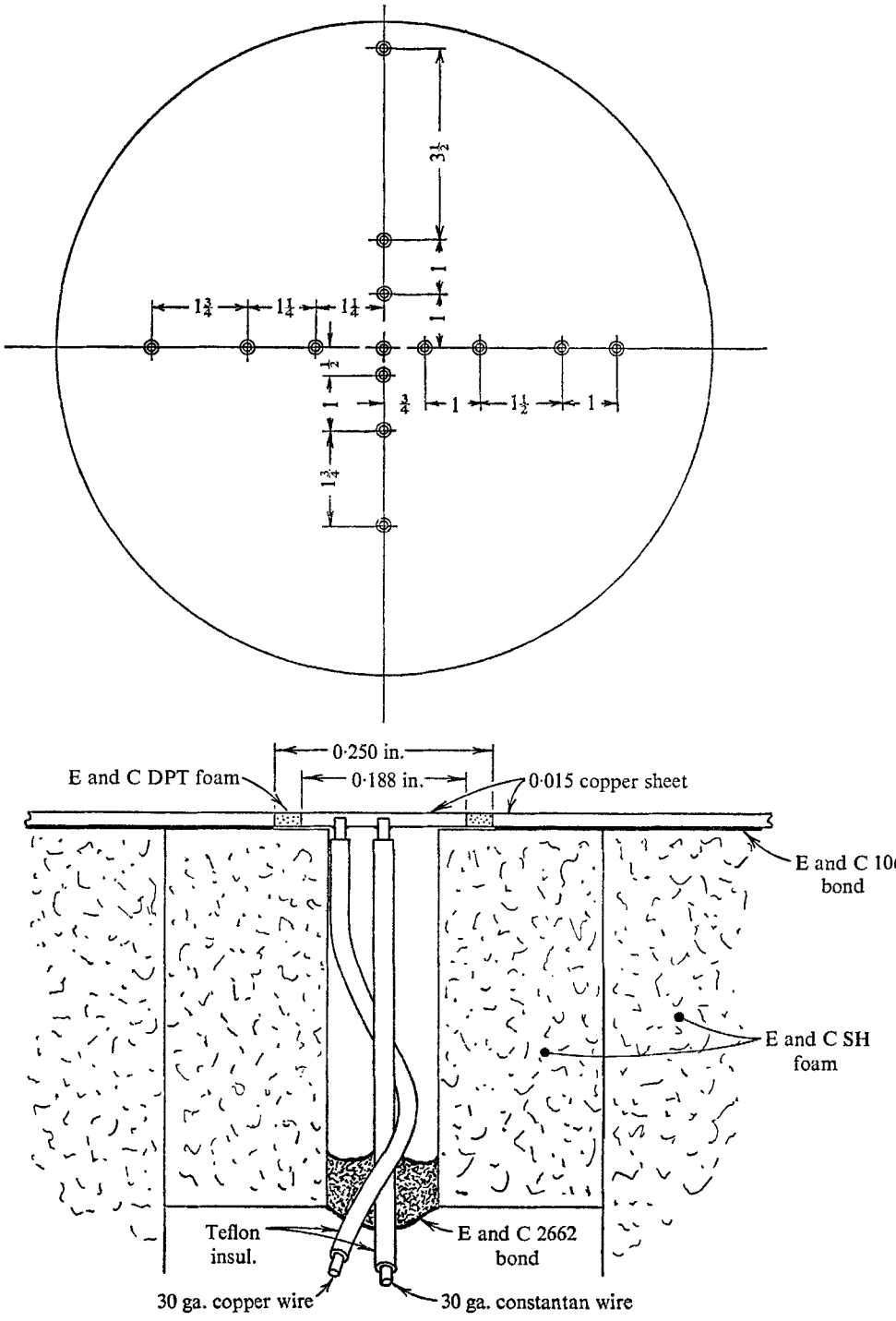

FIGURE 5. Layout of gauges on heat transfer plate and detail of gauge construction.

where m = mass of the gauge disk = 0.060 g; c_p = specific heat of copper; T_w = gauge temperature; T_0 = ambient temperature; $\dot{q}_{\text{in}}$ = unknown heat flux input; h = convective heat transfer coefficient; A_c = area of gauge subjected to convective cooling; A_r = area of gauge subjected to radiative cooling; σ = Boltzmann constant; ϵ = emissivity of gauge (= 1 for lampblack coating).

Using (1) and the measured response dT/dt, the values of $\dot{q}_{\text{in}}$ and h were determined. It was found that the re-radiation heat transfer was negligible.

Having obtained the values of $\dot{q}_{\text{in}}$ and h in the radiant test environment, the mounted gauge was also blackened and mounted at the same point in this environment. The measured response of the mounted gauge (temperature change as a function of time) was found to agree with that computed using (1) within 5 % after 2 sec.

In order to estimate the magnitude of differences among the 14 gauges in the plate without having to calibrate each one separately, three additional gauges were made in the same way and tested in the heat lamp beam. Each gauge was heated by the lamps repeatedly and the response curves were recorded. It was found that the initial slopes of these response curves for each gauge were repeatable within 6, 8, and 12 %. After 10 sec, the magnitudes of the responses were repeatable within 6, 4, and 3 %. A comparison of the average initial slope of all three gauges showed a spread of 11 %. It was assumed that a similar degree of accuracy would be expected for other gauges constructed in this manner.

Procedure for making heat transfer measurements. The impingement heat transfer measurements were made using the following procedure. The heating pad was first brought to a temperature slightly below its maximum operating temperature (450 °F) and then applied to the surface of the test plate. The air jet was started and stabilized at the desired exit velocity. When the plate temperature approached the desired value, usually about 225 °F the recorder paper was started and the jet deflector was put in place. The heating pad was lifted away from the plate and the jet deflector removed about one or 2 sec later. The temperature–time response was then recorded.

3. Experimental results—velocity measurements

3.1. *Free jet measurements*

The results of surveys of the free jet used in this study are presented below. Most of the detailed hot-film surveys of turbulent phenomena were carried out at jet velocities of $\overline{w}_1 = 200$ ft./sec. This resulted in an initial jet Reynolds number Re_d of $5{\cdot}2 \times 10^4$ where $Re_d = \rho_1 w_1 d_N/\mu_1$ with all quantities evaluated at the nozzle exit. Although, as will be seen, spot checks at other velocities showed slight variations of pertinent parameters from the values measured at 200 ft./sec, the Reynolds number was sufficiently high for the surveys made so that the general character of the turbulence did not change with further increase in velocity. Complete jet surveys were made at axial stations z/d_N of 10, 20, 30, 40, and 50. Some other local measurements were made so as to have complete data on certain variables although no detailed surveys were made at these stations. Only certain typical portions of the total amount of data obtained will be given.

Mean quantities. It is instructive to compare the mean flow measurements obtained with the hot-film probe with those obtained with a Pitot tube. Measurements of the latter type are reported in Donaldson & Snedeker (1971).

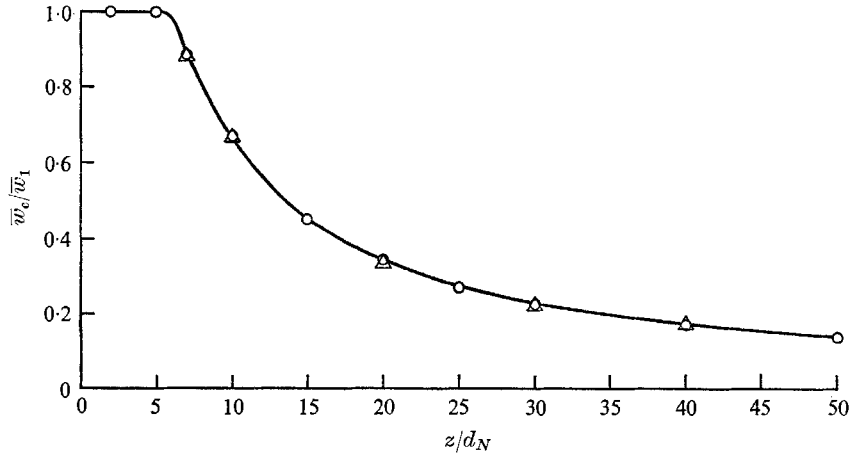

FIGURE 7. Axial decay of jet centreline velocity measured with a Pitot tube and a hot-film X-probe. $\overline{w}_1 = 200$ ft./sec: ○, hot-film X-probe; △, Pitot tube.

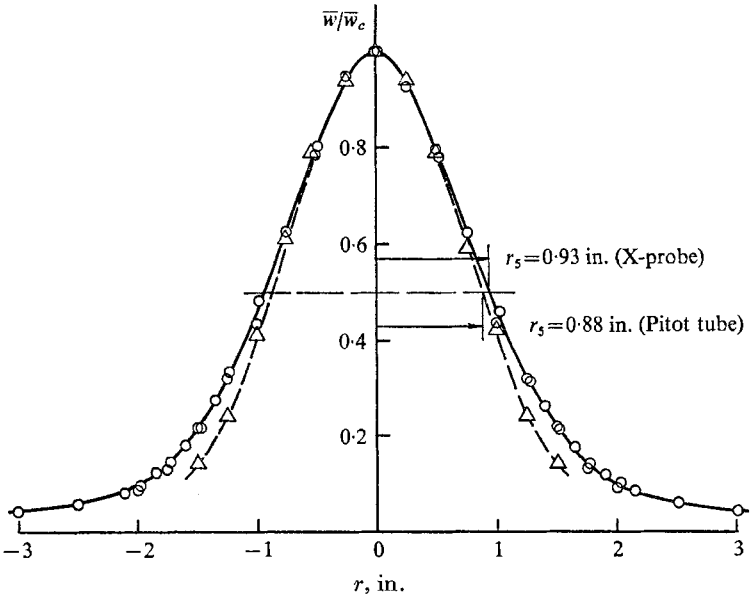

FIGURE 8. Typical free jet velocity profile. $\overline{w}_1 = 200$ ft./sec, $z/d_N = 20$: —○—, hot-film X-probe; – –△– –, Pitot tube.

Figure 7 is a plot of the decay of the mean axial velocity on the centreline of the free jet as a function of distance from the nozzle exit. It may be seen that the agreement between hot-film and Pitot tube measurements of jet centreline velocity is excellent. Figure 8 shows the results of a typical radial survey of axial velocity. Over the central portion of the jet the agreement is also excellent. There is, however, a tendency for the Pitot tube to underestimate the velocities

at the outer edges of the jet. This results, as may be seen, in there being two measured half-radii at a point in a given jet. The difference is not large (only some 5 %). As may be seen from figure 9, which is a plot of jet half-radius as a function of distance from the nozzle, while, typically a Pitot tube defines a narrower half-radius than does a hot-film probe, the half-radii measured in the present studies sometimes fell inside the radius previously defined by Pitot measurement. Such behaviour is, in all probability, indicative of the lack of repeatability of free jet measurements in the same laboratory from one year to the next as a result of subtle changes in the position and shape of nearby laboratory equipment related to the measurements. Finally, and for comparative purposes, the two

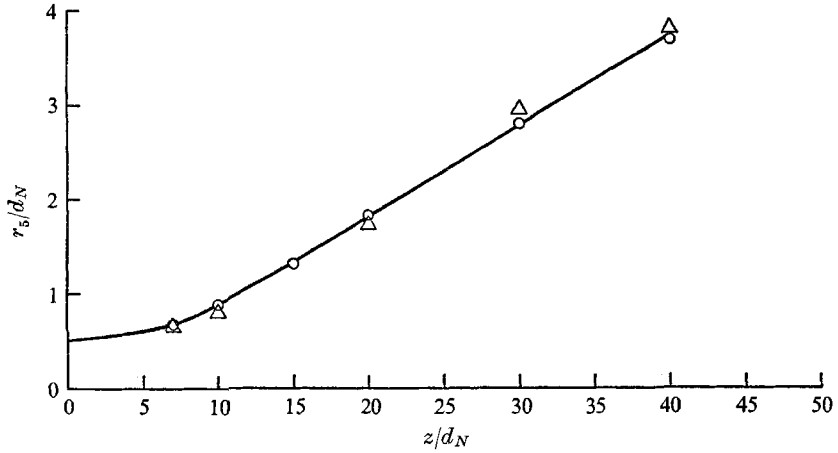

FIGURE 9. Free jet spread as a function of axial distance. $\overline{w}_1 = 200$ ft./sec: ○, hot-film X-probe; △, Pitot tube.

profiles shown in figure 8 are replotted in figure 10 in the non-dimensional form that has been used throughout our studies of jet impingement. For comparison, the commonly used Gaussian velocity profile has been included in this figure.

In the remainder of this paper, the basic reference length r_5 that is used is that obtained from the hot-film measurements.

Turbulent correlations. Figure 11 is a plot of the behaviour of the root-mean-square turbulent velocity fluctuations in the radial and axial directions on the centreline of the free jet. As mentioned previously, most of the data shown were taken at 200 ft./sec, but some data taken at 300 and 500 ft./sec are also included. This figure also shows the results of similar measurements obtained by Corrsin (1943), Corrsin & Uberoi (1950), Laurence (1956), and Gibson (1963). It is seen that the data are, on the whole, in excellent agreement with the results of previous investigations except for the original low Reynolds number data obtained by Corrsin. An interesting point may be made in connexion with the data presented in figure 11. It was observed during these studies that the region just downstream of the core, i.e. the region $10 < z/d_N < 25$, was particularly sensitive, in regard to turbulence levels, to changes in nozzle velocity. Indeed, the small bumps observed in the turbulent intensity curves in this region at 200 ft./sec (which have not been observed by other investigators) may have been due to a slight flapping of the jet being studied.

The one-dimensional spectra of the centreline $\overline{w'^2}$ and $\overline{u'^2}$ just presented were obtained at the five reference stations $z/d_N = 10$, 20, 30, 40, and 50.† The $\overline{w'^2}$ spectra for $z/d_N = 20$, 30, 40, and 50 are plotted in figure 12, while the spectrum for $z/d_N = 10$ is shown in figure 13. Careful comparison of these two figures indicates that turbulent similarity has been achieved at approximately $z/d_N = 20$. At $z/d_N = 10$, although from previous measurements (Donaldson & Snedeker 1971) it was established that similarity of the mean velocity profiles had been

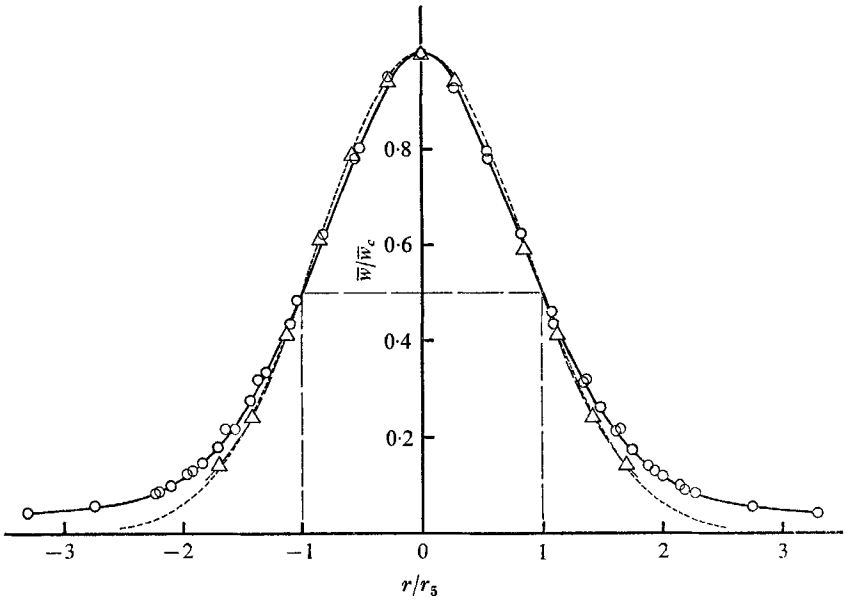

FIGURE 10. Normalized free jet velocity profile. $\overline{w}_1 = 200$ ft./sec, $z/d_N = 20$: —○—, hot-film X-probe; – – △ – –, Pitot tube; - - - - -, Gaussian.

achieved, it is obvious from a comparison of the data in figures 12 and 13 that turbulent similarity is not yet achieved. The $\overline{w'^2}$ spectra obtained in the developed free jet agree well at the lower wave-numbers with a similar spectrum obtained by Gibson (1963). As might be expected, Gibson's data, having been obtained at an order-of-magnitude higher Reynolds number, do not indicate as rapid a fall-off with increasing wave-number as do the present data. Also as expected, Gibson's spectrum exhibits a larger region in which the $-\frac{5}{3}$ power fall-off typical of high Reynolds number turbulent spectra is adhered to.

Radial velocity spectra are shown in figure 14. Again, it appears that the spectrum for $z/d_N = 10$ has not yet achieved similarity. Indeed, the general similarity of spectra for $z/d_N > 10$ is not so pronounced as in the case of the $\overline{w'^2}$ spectra. Some of this lag is due to experimental error, but a portion of the lag is probably due to the longer time taken for the $\overline{u'^2}$ spectra to achieve complete similarity—a result that is expected from theoretical considerations.

† The spectra are presented in the form of normalized power spectra based on the non-dimensional frequency $r_5 k$. Thus

$$F_{\overline{w'^2}}(r_5 k) = \frac{1}{\overline{w'^2}} \frac{\overline{dw'^2}}{d(r_5 k)} \quad \text{and} \quad \int_0^\infty F_{\overline{w'^2}} d(r_5 k) = 1,$$

where $k = 2\pi f / w_c$.

From the $\overline{w'^2}$ spectra just presented, the integral scale L_z of the turbulence on the centreline of a developed free jet may be evaluated from the relation

$$L_z = \tfrac{1}{2}\pi F_{\overline{w'^2}}(0)\cdot r_5, \tag{2}$$

where $F_{\overline{w'^2}}(0)$ is the zero intercept of the non-dimensional spectrum function $F_{\overline{w'^2}}(r_5 k)$. Estimating the zero intercepts of the power spectra shown in figure 10 to be approximately 0·4 results in an integral scale in the developed region of the free jet that is roughly 63 % of the local half-radius of the jet.

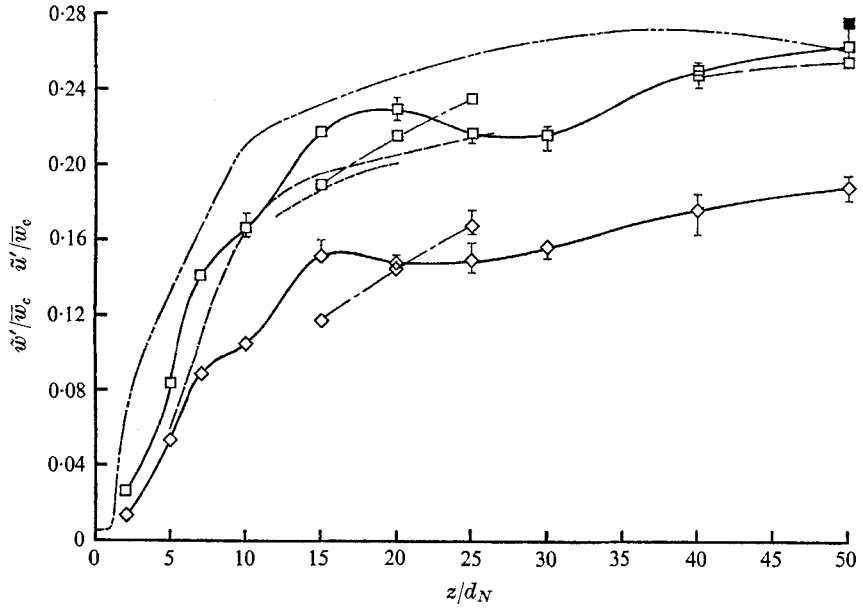

FIGURE 11. Free jet turbulence measured on the centreline.

		$\overline{w}_1$, ft./sec	Re_d
□ $\tilde{w}'/\overline{w}_c$	———	200	$5{\cdot}4\times10^4$
◇ $\tilde{u}'/\overline{w}_c$	— — —	300	$8{\cdot}1\times10^4$
	— — —	500	$1{\cdot}35\times10^5$
■ Gibson (1963)		170	$5{\cdot}4\times10^5$
$\tilde{w}'/\overline{w}_c$	— — — — — — Laurence (1956)	320	$6{\cdot}0\times10^5$
	— — — — Corrsin & Uberoi (1950)	65–115	$3{\cdot}5\times10^4-6{\cdot}1\times10^4$
	— · — Corrsin (1943)	33	$1{\cdot}75\times10^4$

In figures 15 and 16, distributions of the root-mean-square values of $\overline{u'^2}$ and $\overline{w'^2}$ that are typical of a developed jet are plotted. In figure 15, $\tilde{u}'$ and $\tilde{w}'$ are made dimensionless using the local mean velocity $\overline{w}$, while in figure 16 the centreline mean velocity $\overline{w}_c$ is used.† It will be noted in figure 16 that a small dip appears in the magnitude of $\tilde{u}'$ and $\tilde{w}'$ on the axis of the jet. This dip represents

† The root-mean-square turbulent components are defined by $\tilde{u}' = (\overline{u'^2})^{\frac{1}{2}}$, $\tilde{v}' = (\overline{v'^2})^{\frac{1}{2}}$, $\tilde{w}' = (\overline{w'^2})^{\frac{1}{2}}$.

the last vestige of the effect of the core region of the jet, since, in the core, the maximum turbulent velocities are found away from the axis. The disappearance of the dip in the $\tilde{u}'$ and $\tilde{w}'$ distributions may be taken as another indication of the jet having become fully developed at $z/d_N \approx 20$ as has previously been noted by Corrsin (1943).

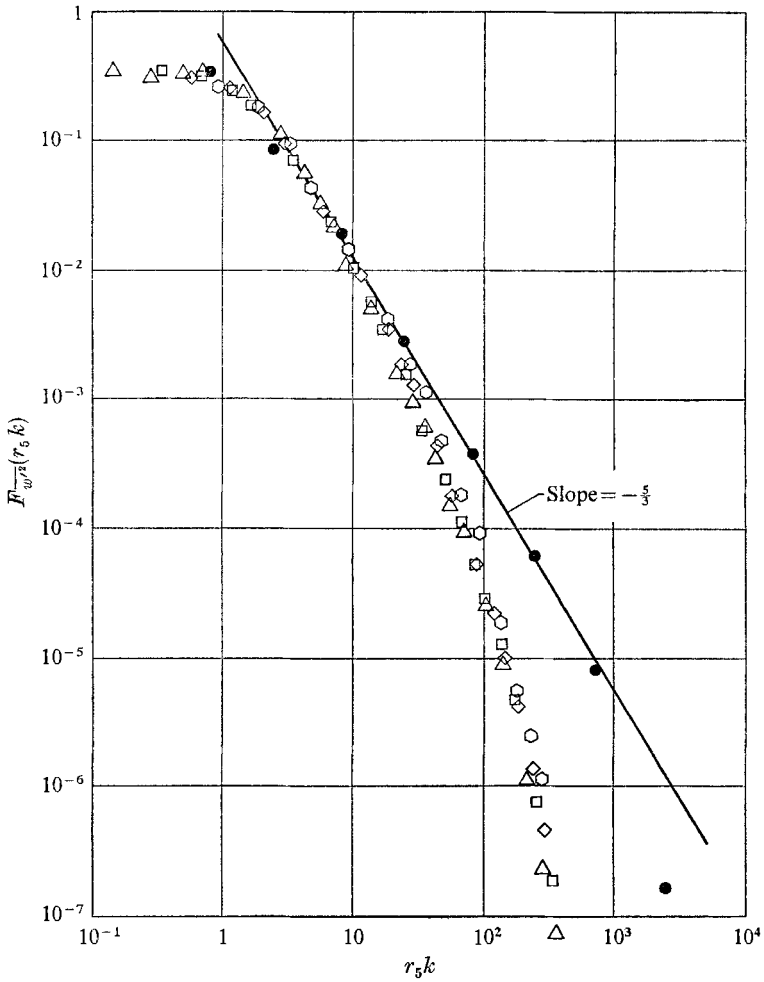

FIGURE 12. Spectra of $\overline{w'^2}$ measured on centreline of free jet. $\overline{w}_1 = 200$ ft./sec. $Re_5 \approx 3 \times 10^4$, values of z/d_N: △, 20; □, 30; ◇, 40; ○, 50. $Re_5 = 3{\cdot}5 \times 10^5$: ●, Gibson (1963).

In figures 17 and 18 a distribution of the turbulent shear correlation $\overline{u'w'}$ across the jet that is typical of the developed region is shown. As before, two methods of making this stress correlation non-dimensional are depicted. In figure 18 the measurements are compared with those of Corrsin (1943) and the agreement is seen to be excellent.

At this point, it can be concluded on the basis of the measurements just presented, that the turbulent characteristics of the free jet used in this study agree well with turbulence measurements made in other free jets. In view of its well-

behaved microstructure, it would appear that the heat transfer measurements that will be reported later should be typical of those that will be found in free jets whose Reynolds numbers are high enough for fully developed turbulent jets to be established.

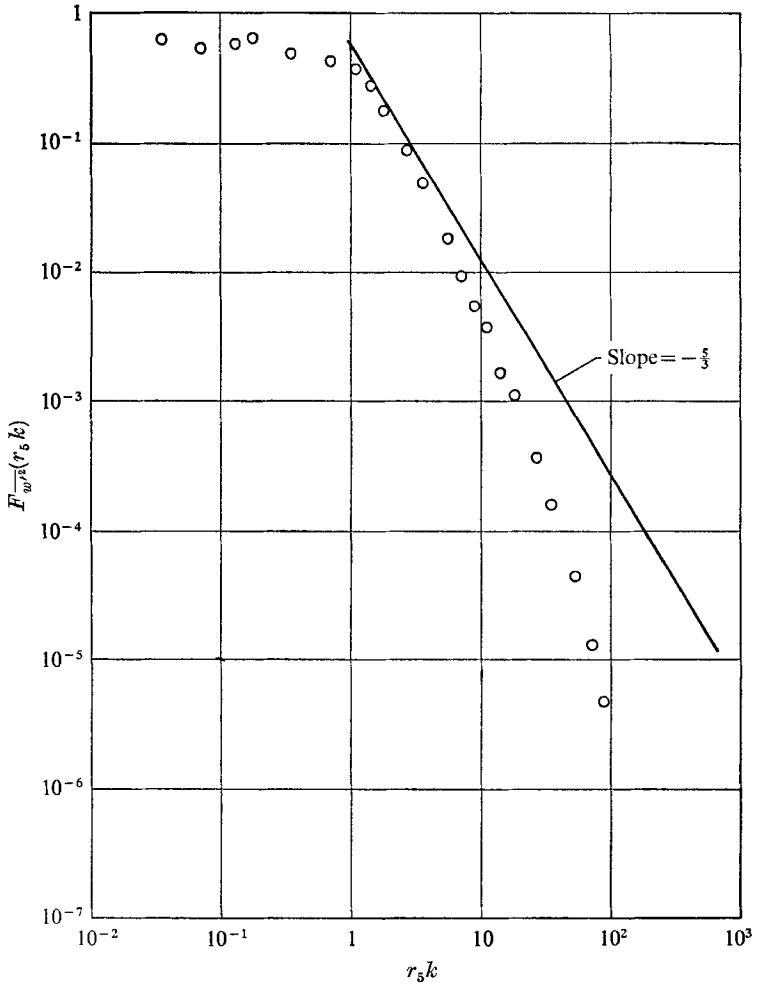

FIGURE 13. Spectra of $\overline{w'^2}$ measured on centreline of free jet. $\overline{w}_1 = 200$ ft./sec: ○, $z/d_N = 10$.

3.2. *Impinging jet measurements*

Before the present tests were run, it was anticipated that the interaction between the free jet and the surface upon which it impinged might cause the jet to flap significantly. If this occurred, not only would the turbulence level in the jet be grossly changed, but the heat transfer and pressure distributions on the plate could no longer be properly related to the characteristics of the free jet in the plane of impingement. In order to check on the possibility of such flapping interactions, detailed measurements of the mean and fluctuating components of velocity just upstream of the impingement plate on the centreline of the jet

were made for $z/d_N = 10$, 20, 30, 40, and 50. All surveys were made for a nozzle velocity of 200 ft./sec. Typical results are given in figure 19 for $z/d_N = 10$. The data are plotted both as a function of z/d_N and as a function of the distance upstream of the plate z' made non-dimensional with the free jet half-radius for $z' = 0$. It was found that at all locations of the impingement plate the mean and turbulent velocities away from the plate approached the values measured in the free jet

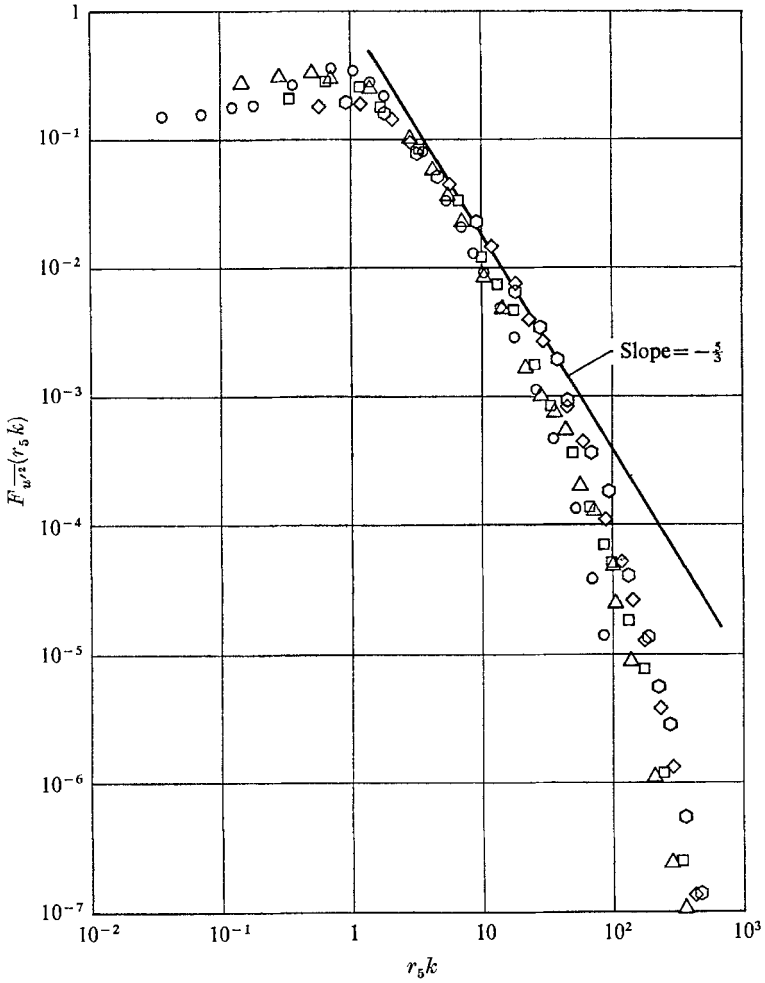

FIGURE 14. Spectra of $\overline{u'^2}$ measured on centreline of free jet. $\bar{w}_1 = 200$ ft./sec. Values of z/d_N: ○, 10; △, 20; □, 30; ◇, 40; ⬡, 50.

closely enough so as to indicate that no serious jet flapping existed. For the case shown, near the core ($z/d_N = 10$), the upstream influence of the plate extends some two jet half-radii which at this location is roughly two nozzle diameters. In the developed jet, the upstream influence becomes fixed at approximately 1·6 jet half-radii.

4. Experimental results—pressure measurements

Before going on to discuss the heat transfer measurements that were made, one more set of measurements which were designed to complete the specifications of the free jet being employed should be presented. Measurements were made of the fluctuations in total pressure on the centreline of the free jet and at the stagnation point of the impingement plate. These measurements were made at $w_1 = 200$ ft./sec for axial positions $z/d_N = 10$, 20, and 30. The non-dimensional spectra of these

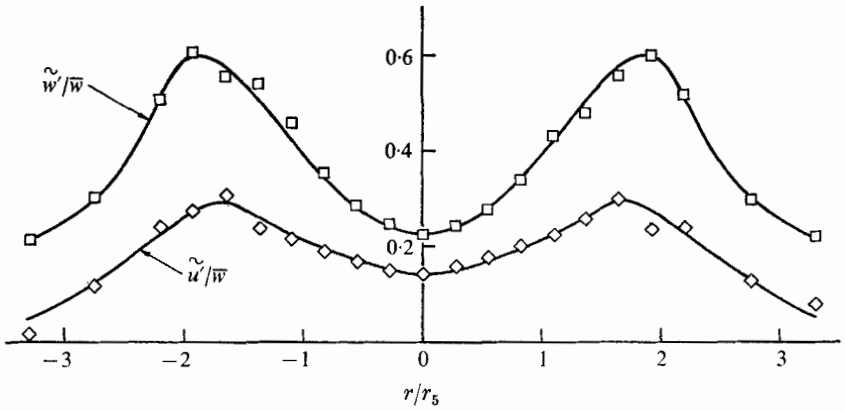

FIGURE 15. Radial distribution of r.m.s. turbulent velocity component in the free jet. $\overline{w}_1 = 200$ ft./sec, $z/d_N = 20$.

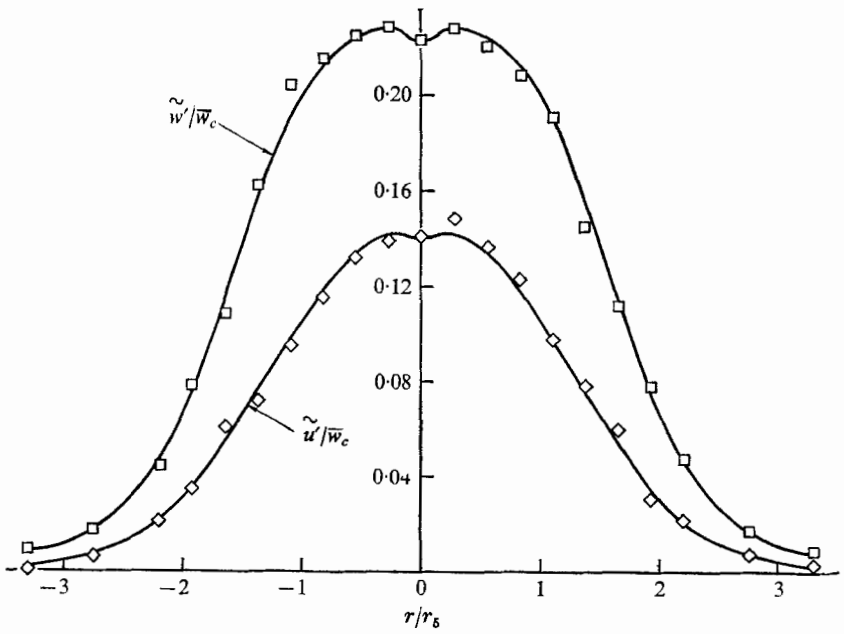

FIGURE 16. Radial distribution of r.m.s. turbulent velocity component in the free jet. $\overline{w}_1 = 200$ ft./sec, $z/d_N = 20$.

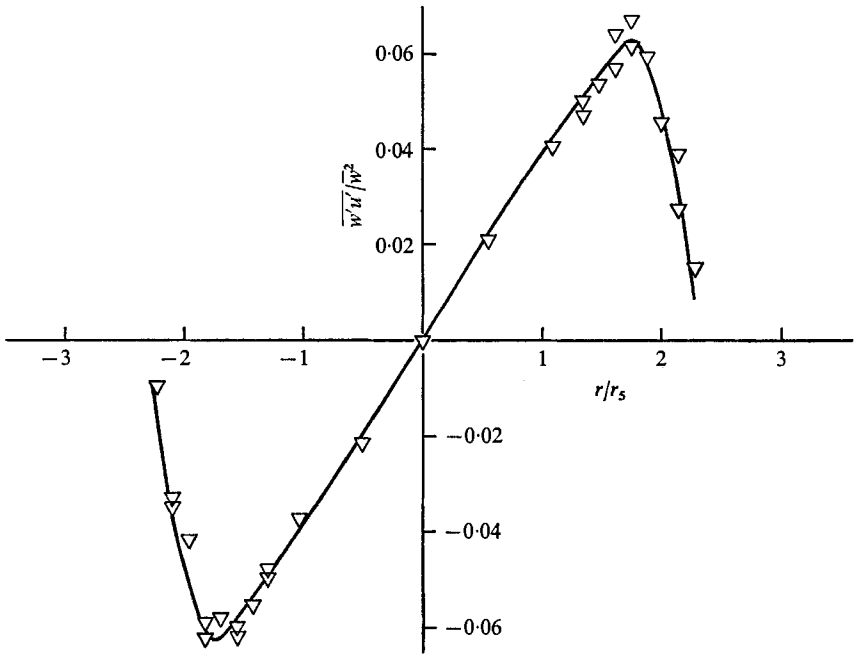

FIGURE 17. Radial distribution of turbulent shear correlation in the free jet. $\overline{w}_1 = 200$ ft./sec, $z/d_N = 20$.

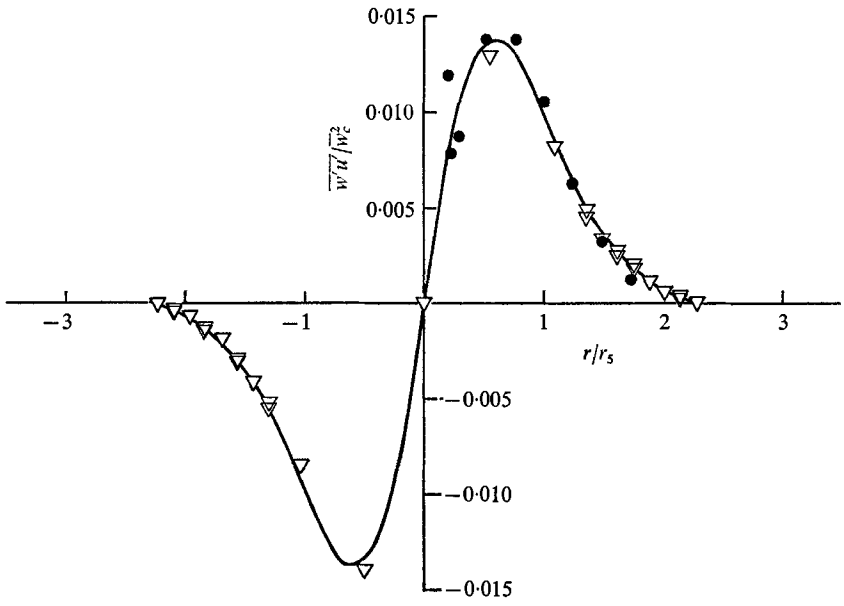

FIGURE 18. Radial distribution of turbulent shear correlation in the free jet. —▽—, present study: $\overline{w}_1 = 200$ ft./sec, $z/d_N = 20$, $Re_d = 5{\cdot}4 \times 10^4$. ●, Corrsin (1943): $\overline{w}_1 = 33$ ft./sec, $z/d_N = 20$, $Re_d = 1{\cdot}7 \times 10^4$.

total pressure fluctuations in the free jet are shown in figure 20.† As in the case of the other turbulent spectra which have been reported, it would appear that total pressure fluctuations also become of similar form for $z/d_N > 20$.‡ The spectra of $\overline{p'^2}$ at the stagnation point of the impingement plate are shown in

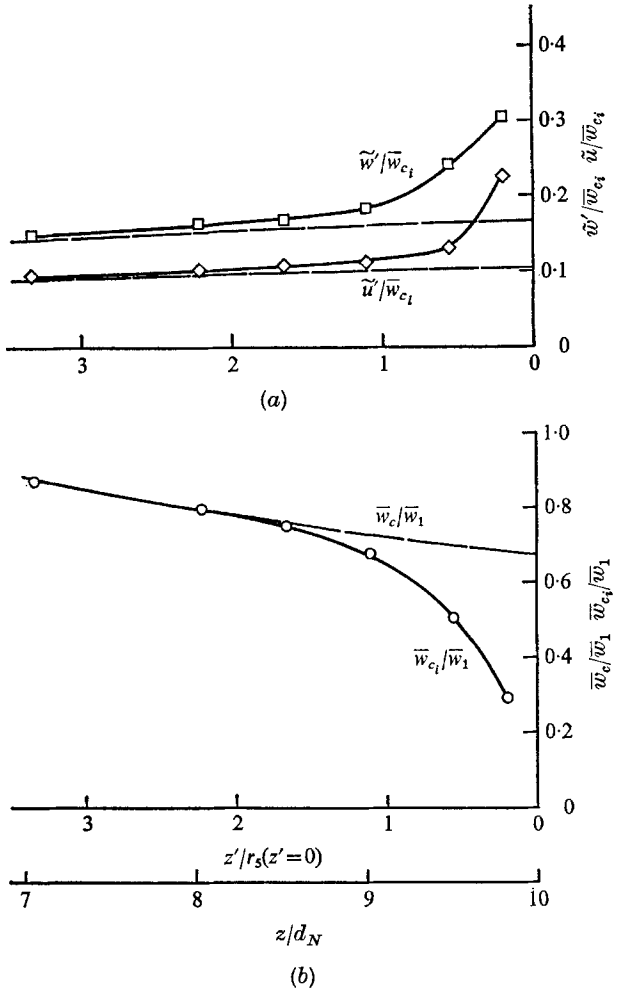

FIGURE 19. Mean and turbulent velocities measured on the centreline upstream of the impingement plate. $z/d_N = 10$. $\overline{w}_1 = 200$ ft./sec. ——, free jet; —□—, —◇—, —○—, impinging jet. The subscript $_i$ indicates values for impinging jet.

figure 21. Here again the spectra appear similar for $z/d_N \geqslant 20$ except for what is felt to be an experimental difficulty at the higher frequencies. It is of some interest to compare these data with the measurements obtained by Strong,

† The instantaneous total pressure is defined as

$$p = \overline{p} + p'$$

and the mean-square total pressure fluctuation is $\overline{p'^2}$.

‡ The lack of similarity of these spectra at the higher wave-numbers is thought to be due to the low signal-to-noise ratio at the higher frequencies.

Siddon & Chu (1967) for a jet of nozzle Reynolds number $Re_d = 2{\cdot}8 \times 10^5$ and at $z/d_N = 7$. While one would not expect these spectra to agree exactly, the general forms of the spectra are similar.

The spectra just presented can be integrated to obtain $\overline{p'^2}/q_c^2$. These non-dimensional total pressure fluctuations are plotted in figure 22 as a function of z/d_N. It is easily seen from these results that the root-mean-square pressure fluctuation at the stagnation point of the impingement plate is roughly 70 % of the r.m.s. total pressure fluctuation in the free jet at an equivalent z/d_N. One may also note the good agreement between the present measurements and those of Strong *et al.* (1967).

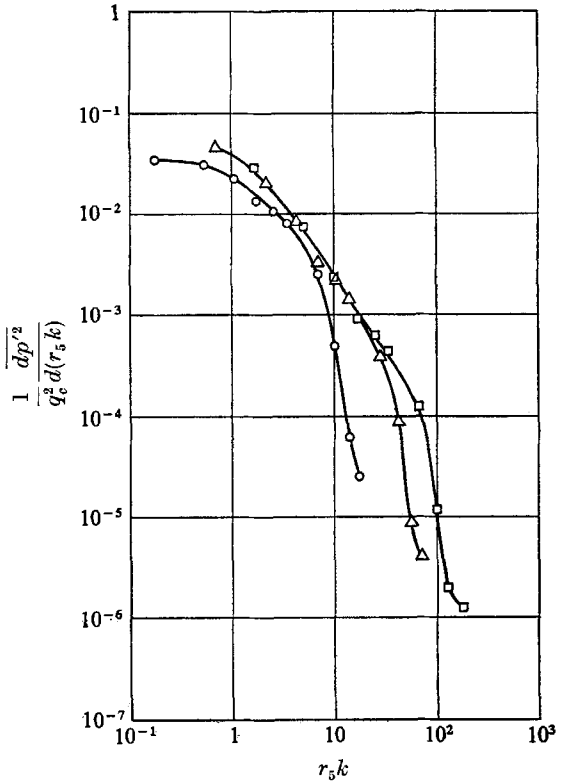

FIGURE 20. Spectra of the fluctuating total pressure on the centreline of the free jet. $\overline{w}_1 = 200$ ft./sec. Values of z/d_N: ○, 10; △, 20; □, 30. The quantity q_c is the local dynamic pressure on the centreline of the free jet.

5. Experimental results—heat transfer

Having presented a fairly detailed description of the free jet used in this study, we now proceed to a discussion of the actual heat transfer measurements. Table 1 indicates the heat-transfer distribution tests which were made. Listed in the table are the nozzle velocities and z/d_N for which measurements were made, together with the pertinent values of local centreline velocity, jet half-radius, and local Reynolds number. Note the approximate constancy of Re_5 with z/d_N

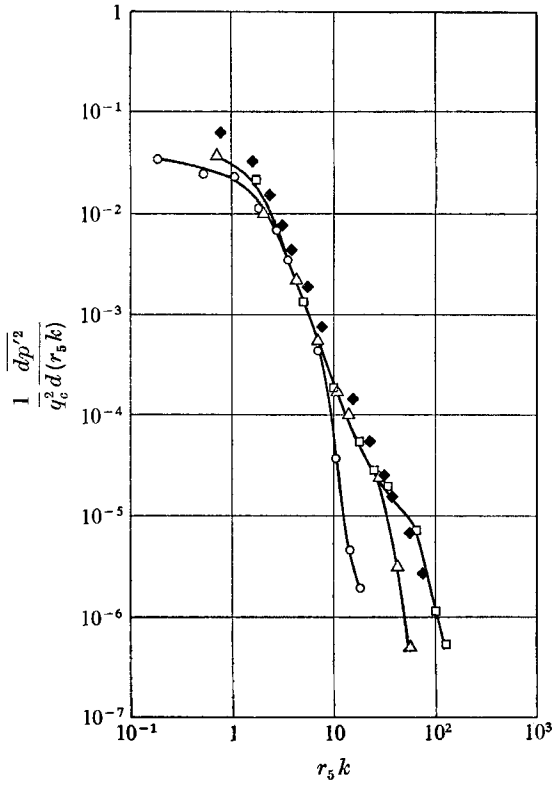

FIGURE 21. Spectra of the fluctuating total pressure at the stagnation point of the impinging jet. $\overline{w}_1 = 200$ ft./sec. Values of z/d_N: ◆, 7 (Strong *et al.* 1967); ○, 10; △, 20; □, 30.

		$\overline{w}_1$, ft./sec			
z/d_N		200	300	500	700
7	$\overline{w}_c =$	177 ft./sec			
	$r_5 =$	0·345 in.	—	—	—
	$Re_5 =$	$3{\cdot}12 \times 10^4$			
10	$\overline{w}_c =$	134	224	401	—
	$r_5 =$	0·450	0·398	0·386	
	$Re_5 =$	$3{\cdot}08 \times 10^4$	$4{\cdot}55 \times 10^4$	$7{\cdot}89 \times 10^4$	
15	$\overline{w}_c =$	90	149	257	—
	$r_5 =$	0·670	0·583	0·572	
	$Re_5 =$	$3{\cdot}16 \times 10^4$	$4{\cdot}44 \times 10^4$	$7{\cdot}51 \times 10^4$	
20	$\overline{w}_c =$	69	109	190	—
	$r_5 =$	0·931	0·838	0·790	
	$Re_5 =$	$3{\cdot}28 \times 10^4$	$4{\cdot}67 \times 10^4$	$7{\cdot}67 \times 10^4$	
30	$\overline{w}_c =$	45	70	120	168
	$r_5 =$	1·43	1·39	1·33	1·30
	$Re_5 =$	$3{\cdot}28 \times 10^4$	$4{\cdot}97 \times 10^4$	$8{\cdot}15 \times 10^4$	$1{\cdot}12 \times 10^5$

TABLE 1

for a fixed nozzle velocity. This constancy is expected in the developed region of the free jet.

Figures 23 and 24 are typical plots of heat transfer distributions on the impingement plate. These particular distributions of film coefficient $h = \dot{q}/\Delta T$ versus

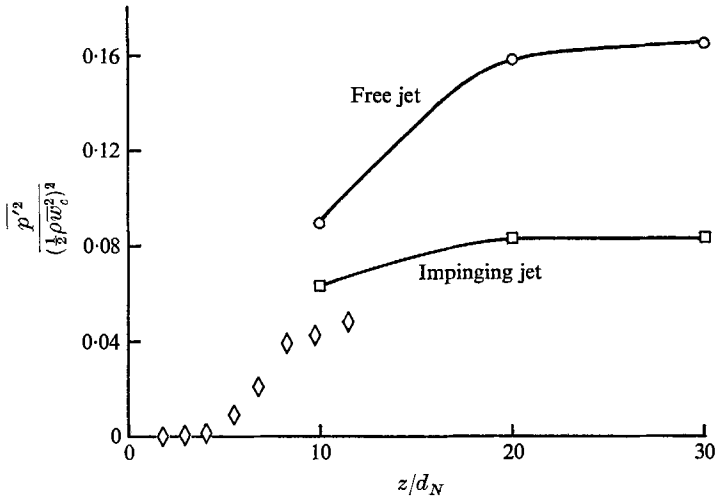

FIGURE 22. Non-dimensional total pressure fluctuations on the centreline of the free and impinging jets. $\overline{w}_1 = 200$ ft./sec. ◇, Strong *et al.* (1967) impinging jet.

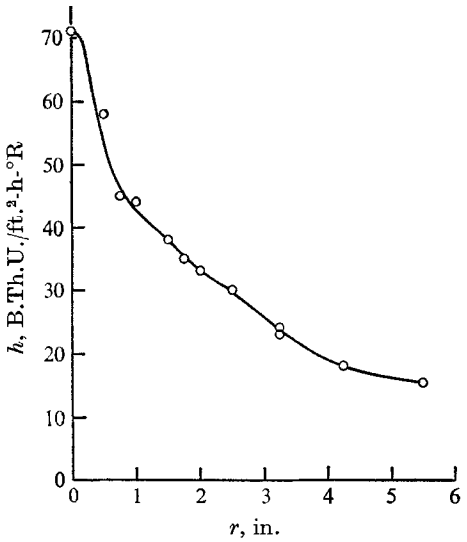

FIGURE 23. Radial distribution of measured film coefficient h for jet impingement on a flat plate. $\overline{w}_1 = 200$ ft./sec, $z/d_N = 10$, $Re_5 = 3{\cdot}08 \times 10^4$.

r have been selected as they were taken at the lowest and highest Reynolds numbers at which tests were made. It will be noted that the general character of these curves follows the behaviour discussed in the introduction, that is, the stagnation point heating is relatively high compared to the wall heating at low Reynolds number, and this ratio becomes smaller as the Reynolds number is

increased. Some liberty has been taken in fairing the curves in figures 23 and 24 as a result of knowledge of the behaviour of the various individual heat gauges gained during the performance of many tests. In general, it was found that the heat transfer near the stagnation point behaved in a manner similar to that of a laminar boundary layer on a surface having the same pressure distribution. The heat transfer rates were, however, a factor of 1·5 to 2 times larger than the calculated laminar values. Away from the stagnation point on the plate, it was found that the heat transfer behaved in a manner similar to a normal turbulent boundary layer which developed in an external flow having a free-stream velocity equal to the local maximum velocity in the wall jet. A more precise statement of this behaviour is given by Rosenbaum & Donaldson (1967) who report a theoretical study done in conjunction with the present experimental study.

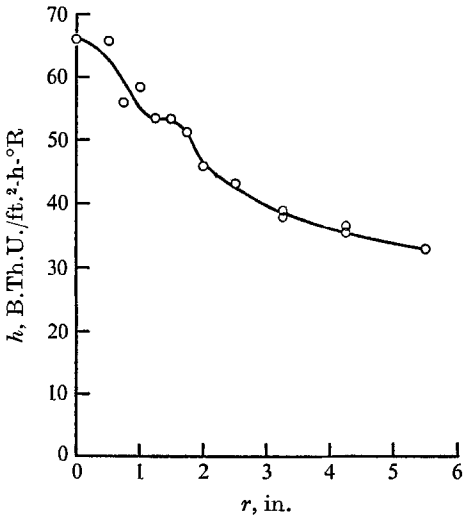

FIGURE 24. Radial distribution of measured film coefficient h for jet impingement on a flat plate. $\overline{w}_1 = 700$ ft./sec, $z/d_N = 30$, $Re_\delta = 11{\cdot}2 \times 10^4$.

Because of the great difference between the behaviour of the heat transfer at and near the stagnation point and in the developed wall jet, it is convenient to discuss the measurements in these regions separately.

5.1. *Stagnation point heat transfer*

In figure 25 the measured stagnation point heat rates made dimensionless by means of the expected laminar heat transfer rates are plotted as functions of z/d_N. The laminar heat transfer rates were obtained from the relation (Lees 1956)

$$\dot{q}_{\text{lam}} = \frac{c_p}{(2Pr)^{\frac{1}{2}}} \left[\rho\mu \left(\frac{du_e}{dr}\right)_{r=0}\right]^{\frac{1}{2}} (T_c^0 - T_w). \tag{3}$$

For the particular conditions at which these tests were run, this relation reduces to

$$\frac{\dot{q}}{\Delta T} = 6{\cdot}95 \times 10^{-1} \left[\left(\frac{du_e}{dr}\right)_{r=0}\right]^{\frac{1}{2}}. \tag{4}$$

For each of the test conditions, the stagnation point velocity gradient $(du_e/dr)_{r=0}$ was evaluated from the data given by Donaldson & Snedeker (1971), and these are the exact values of $\dot{q}_{\text{lam}}$ used in figure 25. Before going on to discuss this figure, it will be useful to note that if the stagnation point velocity gradient is written

$$(du_e/dr)_{r=0} = \alpha \bar{w}_c/r_5, \tag{5}$$

then (3) can be written in the form of a Nusselt number and a Reynolds number based on the local free jet half-radius as

$$Nu_5 = (\tfrac{1}{2}\alpha Pr)^{\frac{1}{2}} (Re_5)^{\frac{1}{2}}, \tag{6}$$

where Pr is the Prandtl number. If α is taken to be the value found for fully developed free jets, namely, $\alpha = 1{\cdot}13$, then for the conditions of these tests

$$Nu_5/(Re_5)^{\frac{1}{2}} = 0{\cdot}635. \tag{7}\dagger$$

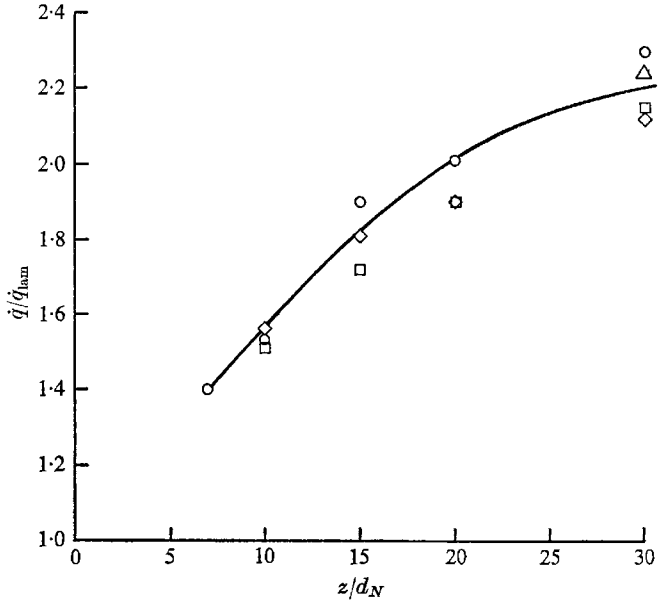

FIGURE 25. Ratio of measured heat transfer to that predicted by laminar theory at the stagnation point of the impinging jet.

$\bar{w}_1$, ft./sec	Approx. Re_5
○ 200	3×10^4
□ 300	5×10^4
◇ 500	8×10^4
△ 700	11×10^4

Returning to figure 25, it may be seen that the stagnation point heat transfer is larger than that predicted for a true laminar flow by a factor that is a function of z/d_N. There does not seem to be any consistent effect of Reynolds number that can be discerned from the data. Comparing figure 25 with figure 11 and noting

† The value $\alpha = 1{\cdot}13$ was found to be approximately valid for any fully developed jet whether it was initially subsonic or supersonic and whether or not it had a shock structure in the core.

the somewhat similar behaviour of the two curves might lead one to suspect that it was the turbulence level in the jet prior to stagnation that was causing the increased laminar heat transfer rates. As mentioned in the introduction, similar increases in stagnation point heat transfer have been measured on spheres and cylinders in flows having approximately homogeneous turbulence produced by grids. In these experiments it has been pointed out that there are two primary parameters that affect the results—the relative turbulent intensity and the ratio of the integral scale of the turbulence to the scale of the body in question. In a free jet, one of these parameters is suppressed since, as has been shown earlier, the ratio of integral scale to the local scale length is a constant.† In view of this,

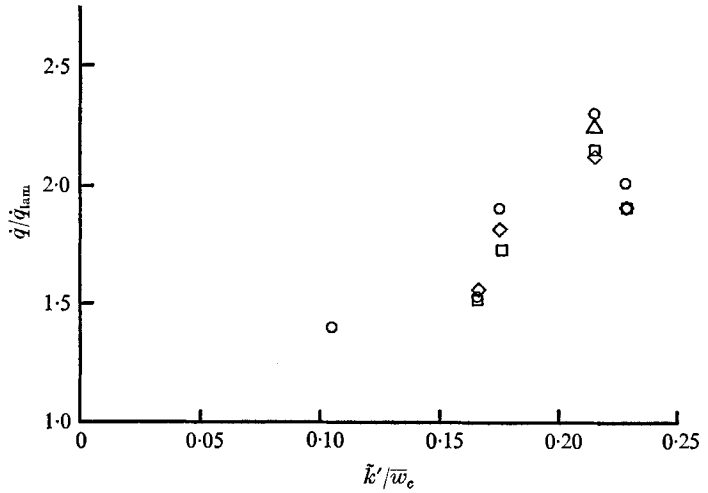

FIGURE 26. Ratio of measured-to-theorectial laminar heat transfer as a function of relative jet turbulent intensity. See figure 25 for list of symbols.

there is shown in figure 26 a plot of $\dot{q}/\dot{q}_{\mathrm{lam}}$ versus the average relative turbulent intensity in the free jet $\tilde{k}'/\overline{w}_e$, where

$$\tilde{k}' = \tfrac{1}{3}(2\overline{u'^2} + \overline{w'^2})^{\frac{1}{2}}. \tag{8}$$

There is seen to be a general increase in $\dot{q}/\dot{q}_{\mathrm{lam}}$ with turbulent intensity, but the scatter of the data at the higher intensities is somewhat large. This scatter is somewhat larger than can be attributed to any one step in arriving at data plotted in figure 26, but perhaps an accumulation of differences can account for the scatter when one considers the problem of going from conditions defined in a free jet to conditions in a given jet impingement. In spite of the scatter evident in figure 26, it is clear that there does not seem to be any strong effect of Reynolds number, that is, an effect which depends on the ratio of the boundary layer thickness at the stagnation point to the scale of the jet itself or its integral scale.

It is of interest to compare the results just presented with the results of recent investigators for the effect of turbulence on heat transfer to cylinders in a uniform turbulent stream. It must be realized that this is not exactly a legitimate com-

† In a fully developed free jet the only local scale length is, of course, the half-radius of the jet.

parison, since it compares results from two-dimensional flow with those of axisymmetric flow, and results from homogeneous turbulence with results from non-homogeneous turbulence. In addition, in one circumstance, the velocity gradient at the stagnation point is caused by body curvature while in the other the same gradient is caused by the rotational velocity profile of the impinging jet. Nevertheless, on figure 27, which is a repetition of the curve given in figure 12 of Smith & Kuethe (1966), we have plotted the results of our measurements. In order to have rough equivalence, the Reynolds number based on diameter, used by Smith & Kuethe, has been replaced by the Reynolds number based on twice the half-radius in plotting the free jet data. It can be seen that the order of magnitude of the effect of turbulence is about the same as has been found by other

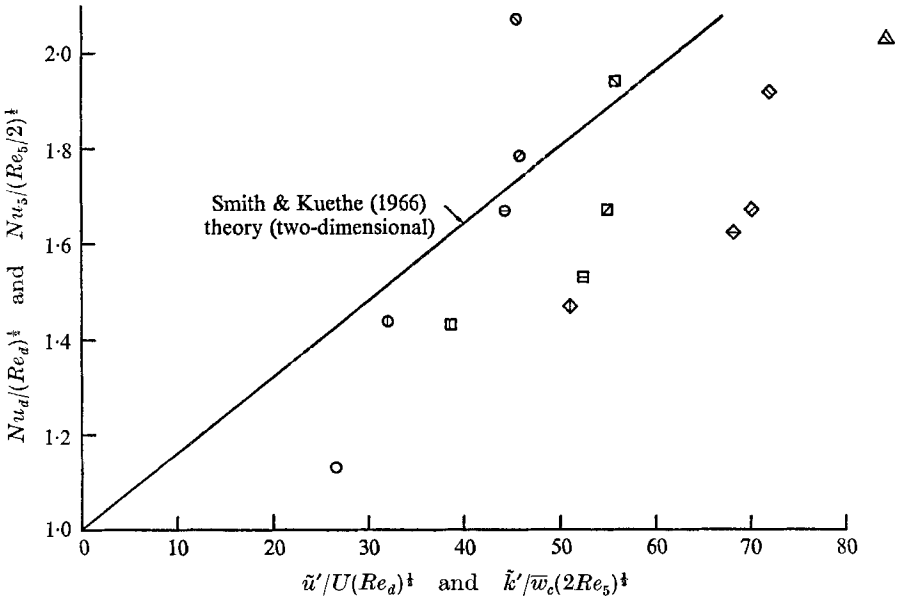

FIGURE 27. Comparison of measured heat transfer for the axisymmetric impinging jet with that predicted by the two-dimensional theory of Smith & Kuethe (1966).

$\overline{w}_1$, ft./sec		z/d_N	
○	200	○	7
□	300	⊙	10
◇	500	⊖	15
△	700	⊘	20
		⦸	30

investigators. In detail, however, the results are quite different. Close examination of the data shows that the effect of Reynolds number is not nearly as pronounced in our axisymmetric free jet results as has been found to be the case for cylinders in uniform turbulent flow.

Before going on to discuss the heat transfer away from the stagnation point, it may be useful to present, in figure 28, a plot of $Nu_5/(Re_5)^{\frac{1}{2}}$ versus Reynolds number, together with the expected accuracy of determining $Nu_5/(Re_5)^{\frac{1}{2}}$ that

results from the measurement of $\dot{q}$ and the evaluation of $\dot{q}_{\text{lam}}$ from measured values of $(du_e/dr)_{r=0}$. It would appear, as has been stated earlier, that there is no discernible effect of Reynolds number.

5.2. *Heat transfer close to the stagnation point*

Close to the stagnation point, the boundary layer behaves as a laminar layer disturbed by having embedded in it the turbulence carried in from the free jet. In the experiments reported here, this region is not well instrumented. The number of heat transfer gauges in this region near the stagnation point was not large, and these gauges proved, unfortunately, to be some of those which had

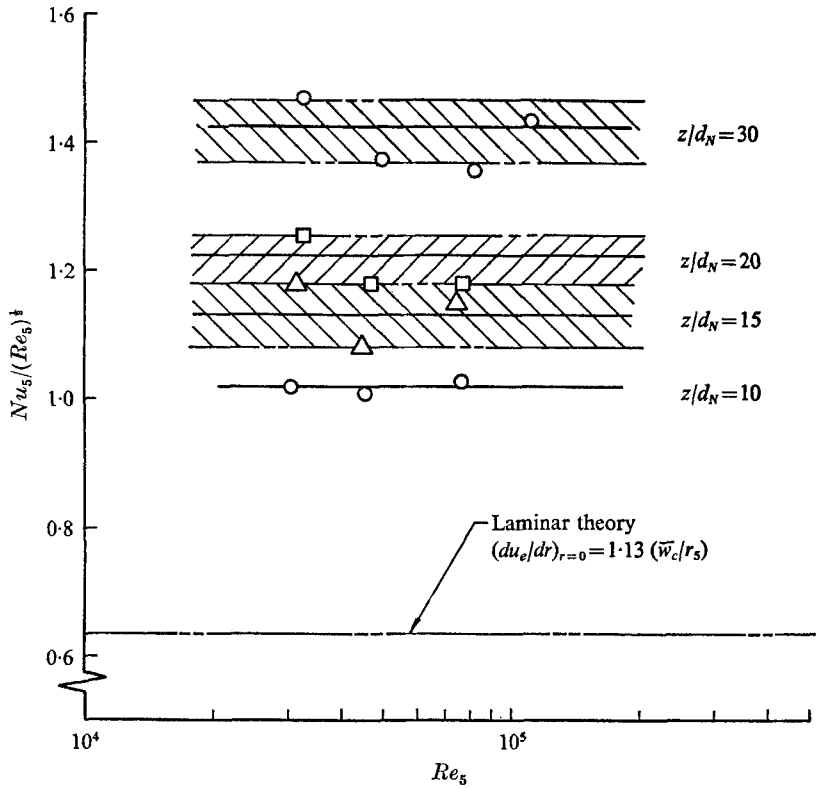

FIGURE 28. Measured heat transfer as a function of local Reynolds number.

large variations from the mean in their behaviour. As a result of these variations, it is difficult to make detailed comments concerning the measured distributions of heat transfer near the stagnation point. It does appear, however, that the actual heat transfers fall off with r/r_5 at a rate slightly greater than that predicted by correcting the normal distribution of laminar heat transfer by a turbulence factor equal to that measured at the stagnation point. This may be seen from an inspection of figure 29 where the measured heat transfers near the stagnation point are compared for the case of $z/d_N = 30$. Although a great deal more work is needed before the exact nature of this near-stagnation point heat transfer

fall-off is understood, it is suggested that, for most engineering computations at large Reynolds numbers, sufficient accuracy will be achieved by applying the stagnation point turbulence correction factor to the normal laminar heat transfer rates in order to estimate local heating near the stagnation point of impinging flows. If such a procedure is followed, it will be found that the heat transfer in the region near the stagnation point will be proportional to the square root of Re_5 and will be a decreasing function of r/r_5 similar to the distributions shown in figure 2.

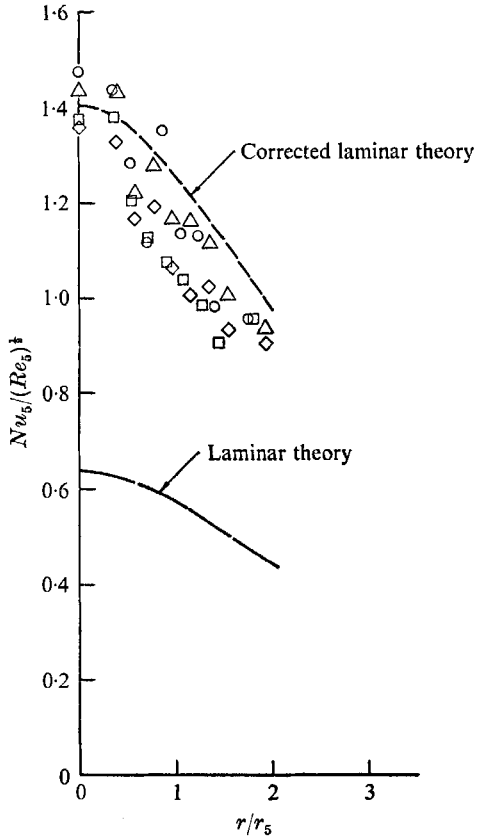

FIGURE 29. Heat transfer close to the stagnation point. $z/d_N = 30$.

$\bar{w}_1$, ft./sec	Re_5
○ 200	$3{\cdot}28 \times 10^4$
□ 300	$4{\cdot}97 \times 10^4$
◇ 500	$8{\cdot}15 \times 10^4$
△ 700	$11{\cdot}15 \times 10^4$

5.3. *Heat transfer far from the stagnation point*

Once transition has occurred in the developing axially symmetric wall jet at a point away from the stagnation point, the behaviour of the heat transfer is quite different from that in the vicinity of $r = 0$. Indeed, based on a simplified analysis of the development of a turbulent boundary layer in a flow whose external velocity falls off as does the maximum velocity in the wall jet, one would expect, at large

distances from the stagnation point, i.e. $r/r_5 \gg 1$, that the Nusselt number based on the length r would be proportional to the eight-tenths power of the Reynolds number based on r_5, namely

$$Nu = \dot{q}r/k\Delta T = \text{const.}\,(Re_5)^{0.8}, \tag{9}$$

or, if $Nu_5 = \dot{q}r_5/k\Delta T$,

$$Nu_5/(Re_5)^{0.8} = \text{const.}\,r_5/r. \tag{10}$$

In view of this relation for $r/r_5 \gg 1$, we might expect a generalization of (10) for smaller r/r_5 to be of the form

$$Nu_5/(Re_5)^{0.8} = f(r/r_5). \tag{11}$$

In figures 30 to 33, the measured heat transfer distributions have been plotted in the form indicated by (11) namely, as Nu_5 as a function of r/r_5. It should be noted that the scatter of the data is largest in figure 30 and, in particular, for

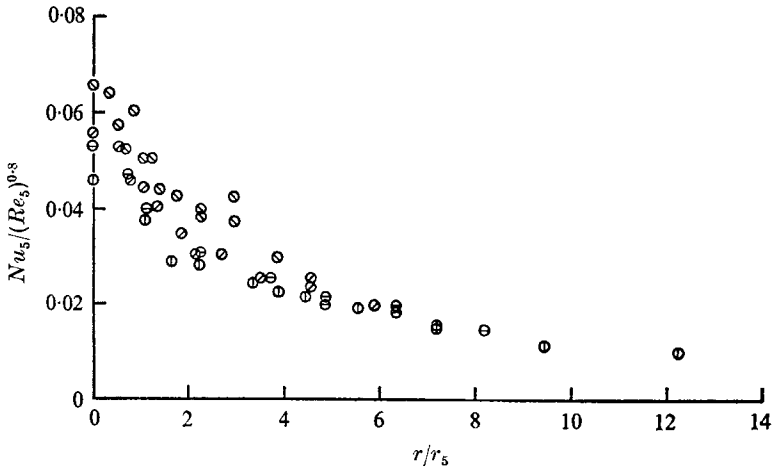

FIGURE 30. Measured heat transfer distribution with $Nu_5 = hr_5/k$. $\overline{w}_1 = 200$ ft./sec, approx. $Re_5 = 3 \times 10^4$. See figure 27 for values of z/d_N.

the cases of z/d_N of 20 and 30. These conditions represented the lowest heat transfer rates measured and are those for which the experimental errors are largest. As the Reynolds number was increased and the general level of heat transfer increased, the scatter in the data decreased (see figures 31 to 33).

When the data are plotted as in figures 30 to 33 for a fixed Reynolds number, only one curve of Nu_5 versus r/r_5 should result at $r/r_5 \gg 1$. Thus, the data scatter at large r/r_5 (say, $r/r_5 > 2$) in these figures is truly a measure of experimental accuracy which for low velocity and large z/d_N was poor. On the other hand, when all the data for different Reynolds numbers are plotted together, as in figure 34, the fact that for r/r_5 equal to approximately 2 or greater all the data fall close to one curve indicates that a relationship such as that given in (11) is valid.

Rosenbaum & Donaldson (1967) have derived a theoretical expression for the turbulent heat transfer below an impinging jet. Their result for the case when Reynolds analogy is assumed to hold is plotted in figure 34 for reference.

The success of the simple correlation suggested by (11) encourages one to attempt a correlation of the form given in (9) in order to obtain a description of the behaviour of jet impingement heat transfer at large r/r_5. Figure 35 is the result of plotting our measurements in this form. As before, one sees a more pronounced scatter in the data at low speeds and large z/d_N. In addition, the

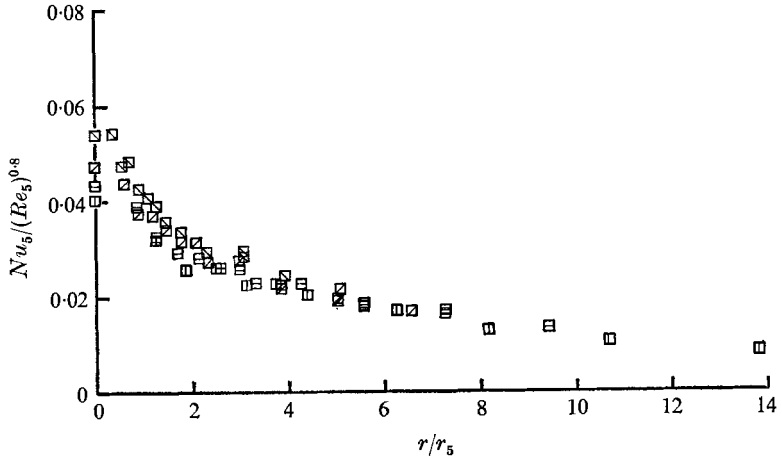

FIGURE 31. Measured heat transfer distribution with $Nu_5 = hr_5/k$. $\bar{w}_1 = 300$ ft./sec, approx. $Re_5 = 5 \times 10^4$. See figure 27 for values of z/d_N.

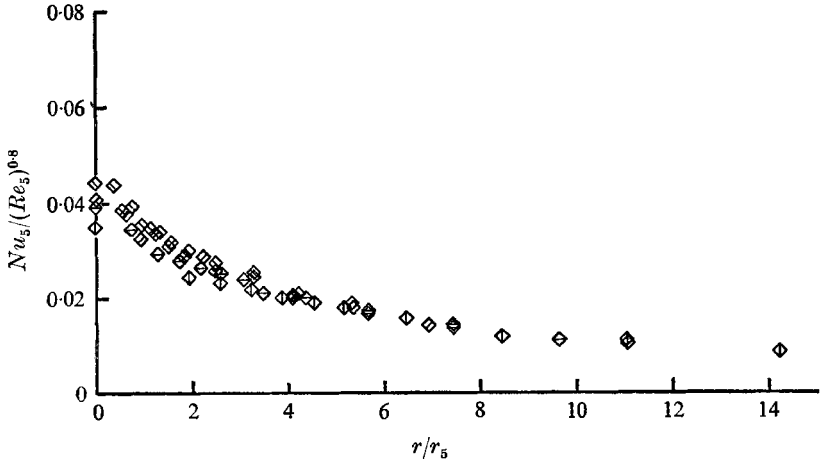

FIGURE 32. Measured heat transfer distribution with $Nu_5 = hr_5/k$. $\bar{w}_1 = 500$ ft./sec, approx. $Re_5 = 8 \times 10^4$. See figure 27 for values of z/d_N.

only data which yield information concerning the large r/r_5 behaviour of the parameter $Nu/(Re_5)^{0·8}$ are those taken at $z/d_N = 10$ and 15. Inspection of the data does indicate, however, that an asymptote may be approached at large r/r_5. Further investigation is needed, but on the basis of present data it would appear that heat transfers at large r/r_5 ($\gtrsim 10$) might be computed on the basis of the following formula:

$$Nu = \dot{q}r/k\Delta T = 0{\cdot}12(Re_5)^{0·8}. \tag{12}$$

5.4. *Comparison with other results*

In general, the heat transfer results obtained in this study agree well with the results of other investigators. It will, perhaps, suffice to compare our results with those of Gardon & Cobonpue (1961). In the upper part of figure 36, a comparison is made of radial heat transfer distributions for the most nearly

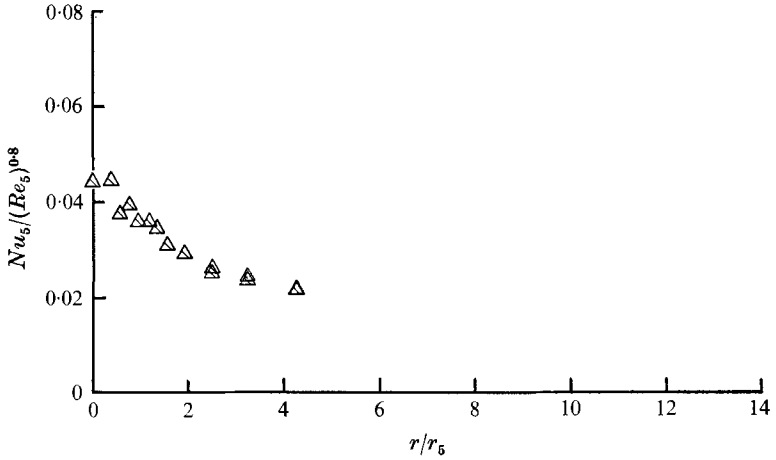

FIGURE 33. Measured heat transfer distribution with $Nu_5 = hr_5/k$. $\bar{w}_1 = 700$ ft./sec, approx. $Re_5 = 11 \times 10^4$. See figure 27 for value of z/d_N.

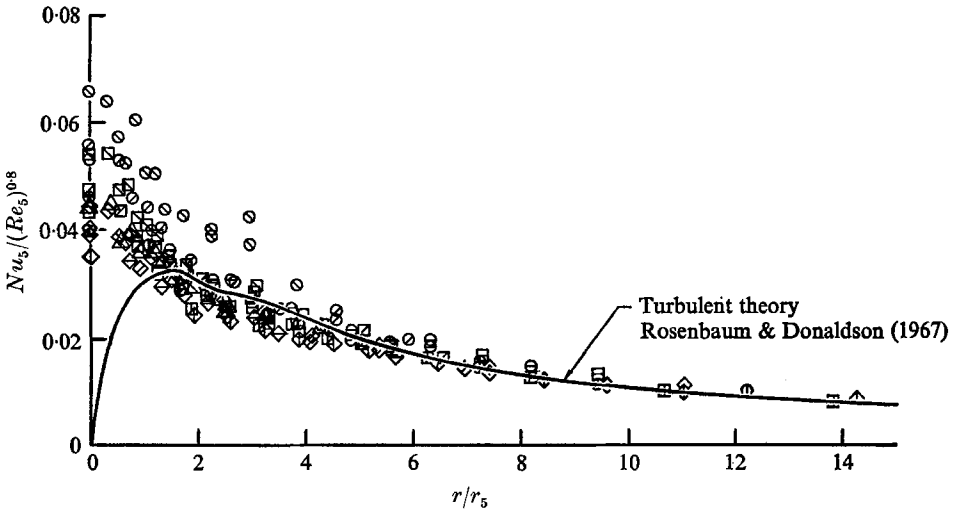

FIGURE 34. Comparison of measured heat transfer data for all Reynolds numbers. See figure 35 for definition of symbols.

equivalent conditions. It is seen that the agreement is excellent. The lower portion of figure 36 shows the axial variation of $\dot{q}/\dot{q}_{\text{lam}}$. In this case the agreement at the two downstream stations is not good, with the values of $\dot{q}/\dot{q}_{\text{lam}}$ measured by Gardon & Cobonpue falling some 27 % below those of the present study. At present the reason for this disagreement is not understood.

6. Conclusions

It was the purpose of the present investigation to develop a rationale for computing the heat transfer that results when a jet impinges on a surface. It appears from the results just presented that the following procedure should yield results that will suffice for most engineering purposes.

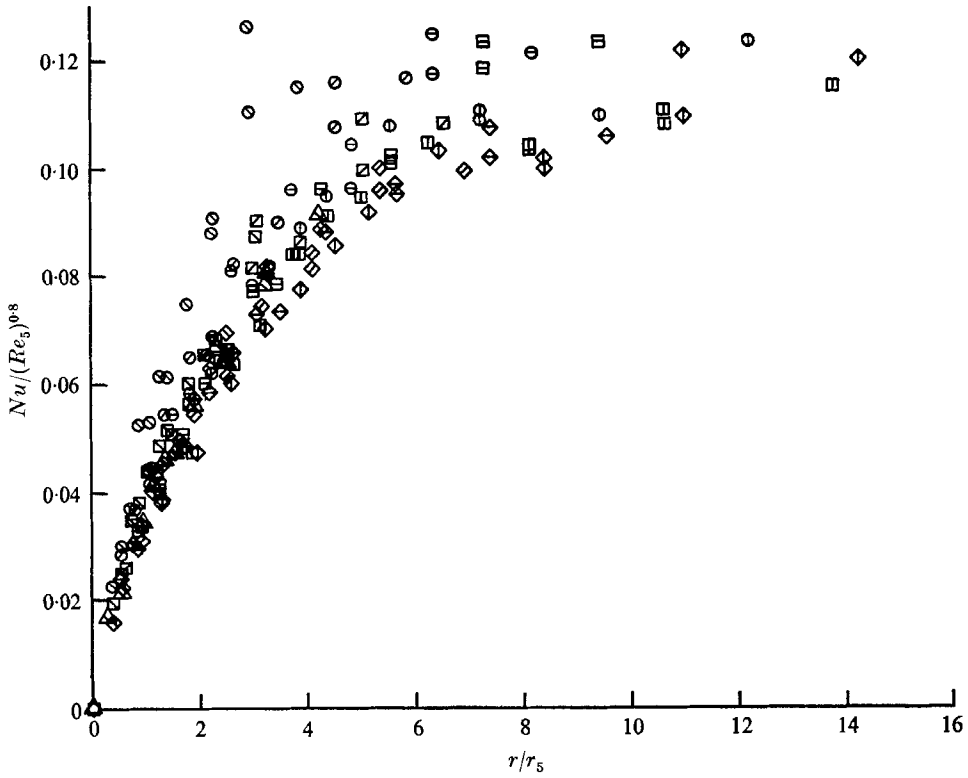

FIGURE 35. Measured heat transfer distribution with $Nu = hr/k$.

	$\overline{w}_1$, ft./sec			
z/d_N	200	300	500	700
10	⊙	⊞	◇	
15	⊖	⊟	◈	
20	⊘	⊠	◈	
30	⊗	⊠	◇	△
Approx. Re_5	3×10^4	5×10^4	8×10^4	11×10^4

In the region near the stagnation point, the heat transfer should be computed by first computing the laminar heat transfer that would take place on a surface having the same pressure distribution as that on the impingement plate. A constant correction factor is then to be applied to these results to account for the structure of the turbulent jet. The appropriate correction factor, which is a

function of z/d_N and not of Reynolds number, is to be obtained from the results given in figure 25.

Farther away from the stagnation point, the heat transfer should be computed on the basis of the technique given by Rosenbaum & Donaldson (1967) and plotted in figure 34.

At most Reynolds numbers of interest, where transition occurs close to the stagnation point, adequate results will be obtained by assuming the larger of these two results to be the proper local heat transfer rate.

Very far from the stagnation point, it appears that the heat transfer film

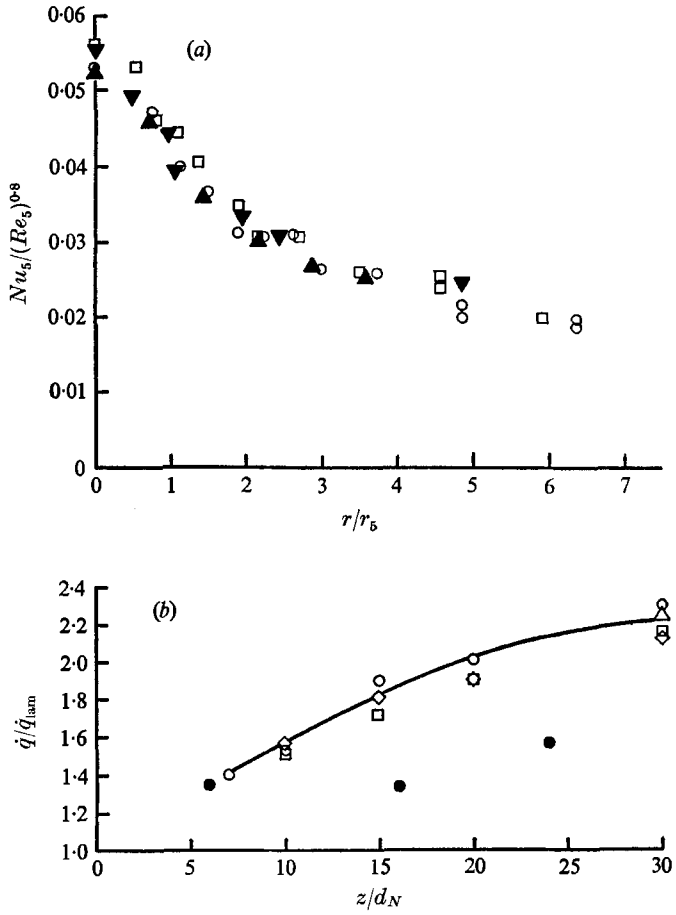

FIGURE 36. Comparison of heat transfer data with those of Gardon & Cobonpue (1961).

(*a*)	z/d_N	Approx. Re_5
	○ 15	3×10^4
	□ 20	3×10^4
	▲ 16	$1{\cdot}6 \times 10^4$ } Gardon & Cobonpue
	▼ 24	$1{\cdot}6 \times 10^4$ } (1961)

(*b*) Approx. Re_5: ○, 3×10^4; □, 5×10^4; ◇, 8×10^4; △, 11×10^4; ●, $1{\cdot}6 \times 10^4$, Gardon & Cobonpue (1961).

coefficient falls off as $1/r$, and for large r/r_5 the heat transfer may be estimated from the approximate formula

$$Nu = \dot{q}r/k\Delta T = 0{\cdot}12(Re_5)^{0{\cdot}8}.$$

The procedures outlined above were developed from measurements of the heat transfer between an impinging jet of air and a heated flat plate. The heat transfer distributions on the plate were measured with thin calorimeters distributed on the surface. Jets having exit velocities of 200, 300, 500, and 700 ft./sec were used. The turbulence characteristics of the same free jets were measured and used as the basis for the correction factors to be applied to the computed laminar stagnation point heating. While the turbulence characteristics were found to agree in general with those measured by others, certain features of the detailed structure were felt to be characteristic of the particular apparatus. For example, it was observed that the turbulence intensity on the centreline of the 200 ft./sec jet reached a maximum at $z/d_N \approx 20$ and then decreased before starting to increase once again at $z/d_N = 30$. Measured turbulent spectra for these jets showed the expected characteristic $-\frac{5}{3}$ drop-off with increasing wave-number, although this behaviour was confined to a small range due to the relatively low Reynolds numbers of the jets.

REFERENCES

Comings, E. W., Clapp, J. T. & Taylor, J. F. 1948 *Ind. Engng Chem.* **40**, 1076.

Corrsin, S. 1943 *NACA ACR* 3L23.

Corrsin, S. & Uberoi, M. S. 1950 *NACA Rep.* 998.

Donaldson, C. duP. & Snedeker, R. S. 1971 *J. Fluid Mech.* **45**, 281.

Gardon, R. & Cobonpue, J. 1961 *Proc.* 1961 *Int. Heat Transfer Conf.* 454.

Gardon, R. & Akfirat, J. C. 1965*a* *ASME Paper* no. 65-HT-20.

Gardon, R. & Akfirat, J. C. 1965*b* *Int. J. Heat Mass Transfer*, **8**, 1261–1272.

Gibson, M. M. 1963 *J. Fluid Mech.* **15**, 161.

Giedt, W. H. 1949 *Trans. ASME* **71**, 375.

Huang, G. C. 1963 *J. Heat Transfer*, **85**, 237.

Kestin, J., Maeder, P. F. & Sogin, H. H. 1961 *Z. angew. Math. Phys.* **12**, 115.

Laurence, J. C. 1956 *NACA Rep.* 1292.

Lees, L. 1956 *Jet Propulsion*, **26**, 4.

Maisel, D. S. & Sherwood, T. K. 1950 *Chem. Engng Prog.* **46**, 131.

O'Connor, T. J., Comfort, E. H. & Cass, L. A. 1965 *AVCO Corp. Tech. Rep.* RAD-TR-65-18.

Reiber, H. 1925 *Mitt. Forschungsarbeiten*, **269**, 1.

Rosenbaum, H. & Donaldson, C. duP. 1967 *Aero. Res. Associates of Princeton, Inc. Rep.* 101.

Schnautz, J. H. 1958 Ph.D. Thesis, Oregon State University.

Seban, R. H. 1960 *J. Heat Transfer*, **82**, 101.

Smith, M. C. & Kuethe, A. M. 1966 *Phys. Fluids*, **9**, 2337.

Strong, D. R., Siddon, T. E. & Chu, W. T. 1967 *UTIA Tech. Note* 107.

van der Hegge Zijnen, B. G. 1957 *Appl. Sci. Res.* A **7**, 205.

Vickers, J. M. F. 1959 *Ind. Engng Chem.* **51**, 967.

Wehofer, S. 1963 *AEDC Tech. Doc. Rep.* 63–93.

Westkaemper, J. C. 1960 *AEDC Tech. Note* 60–202.

Westkaemper, J. C. 1961 *J. Aero. Sci.* **28**, 907.

Zapp, G. M. 1950 MSE Thesis, Oregon State University.

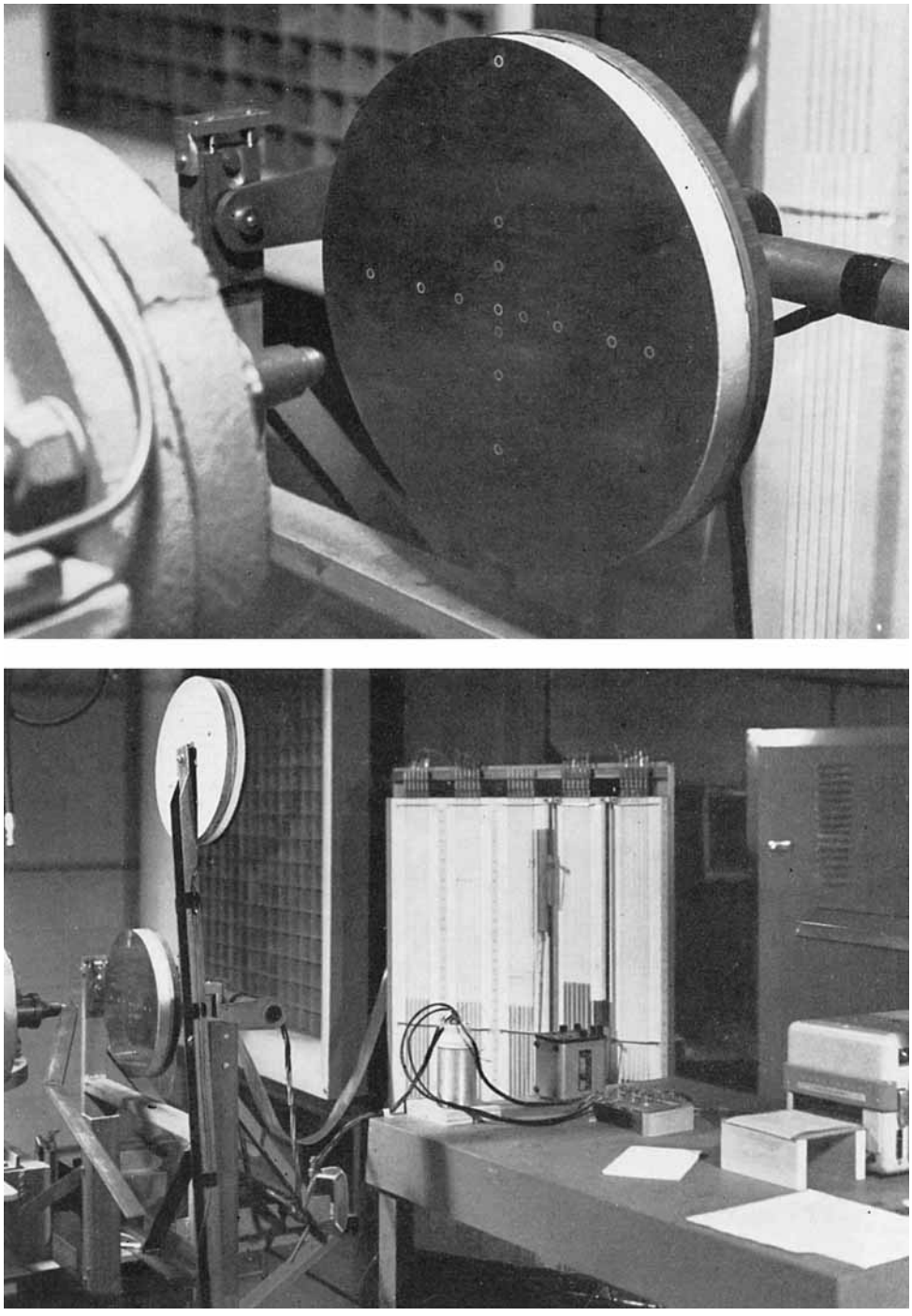

FIGURE 6. Views of the heat transfer apparatus.